Theses and Dissertations | 1. Thesis and Dissertation Collection, all items

1988-03

An objective technique for Arctic cloud analysis using multispectral AVHRR satellite imagery

Barron, John P.

Monterey, California. Naval Postgraduate School

http://hdl.handle.net/10945/23335

NAVAL POSTGRADUATE SCHOOL
Monterey , California

THESIS

AN OBJECTIVE TECHNIQUE FOR ARCTIC CLOUD
ANALYSIS
USING MULTISPECTRAL AVHRR SATELLITE
IMAGERY

by

John P. Barron

March 1988

Thesis Advisor	Philip A. Durkee
Co-Advisor	Carlyle H. Wash

Approved for public release; distribution is unlimited.

REPORT DOCUMENTATION PAGE

1a. REPORT SECURITY CLASSIFICATION Unclassified		1b RESTRICTIVE MARKINGS		
2a. SECURITY CLASSIFICATION AUTHORITY		3 DISTRIBUTION / AVAILABILITY OF REPORT Approved for public release; distribution is unlimited.		
2b. DECLASSIFICATION / DOWNGRADING SCHEDULE				
4. PERFORMING ORGANIZATION REPORT NUMBER(S)		5 MONITORING ORGANIZATION REPORT NUMBER(S)		
6a. NAME OF PERFORMING ORGANIZATION Naval Postgraduate School	6b. OFFICE SYMBOL (If applicable) 63	7a NAME OF MONITORING ORGANIZATION Naval Postgraduate School		
6c. ADDRESS (City, State, and ZIP Code) Monterey, CA 93943-5000		7b. ADDRESS (City, State, and ZIP Code) Monterey, CA 93943-5000		
8a. NAME OF FUNDING / SPONSORING ORGANIZATION	8b OFFICE SYMBOL (If applicable)	9. PROCUREMENT INSTRUMENT IDENTIFICATION NUMBER		
8c. ADDRESS (City, State, and ZIP Code)		10. SOURCE OF FUNDING NUMBERS		
		PROGRAM ELEMENT NO	PROJECT NO.	TASK NO	WORK UNIT ACCESSION NO

11. TITLE (Include Security Classification)
AN OBJECTIVE TECHNIQUE FOR ARCTIC CLOUD ANALYSIS USING MULTISPECTRAL AVHRR SATELLITE IMAGERY

12. PERSONAL AUTHOR(S)
Barron, John P.

13a. TYPE OF REPORT Master's Thesis	13b. TIME COVERED FROM _____ TO _____	14. DATE OF REPORT (Year, Month, Day) 1988 March	15 PAGE COUNT 81

16. SUPPLEMENTARY NOTATION

17. COSATI CODES			18 SUBJECT TERMS (Continue on reverse if necessary and identify by block number)
FIELD	GROUP	SUB-GROUP	arctic cloud analysis, AVHRR channel 3, snow/cloud discrimination

19. ABSTRACT (Continue on reverse if necessary and identify by block number)

An established cloud analysis routine has been modified for use in the Arctic. The separation of clouds from the snow and sea ice backgrounds is accomplished through a multispectral technique which utilizes AVHRR channel 2 (visible), channel 3 (near infrared) and channel 4 (infrared) data. The primary means of cloud identification is based on a derived channel 3 reflectance image. At this wavelength, a significant contrast exists between liquid clouds and the arctic backgrounds, unlike in the standard visible and infrared images. The channel 3 reflectance is obtained by first using the channel 4 emission temperature to estimate the thermal emission component of the total channel 3 radiance. This thermal emission component is subsequently removed from the total radiance, leaving only the solar reflectance component available for analysis. Since many ice clouds do not exhibit

20 DISTRIBUTION / AVAILABILITY OF ABSTRACT ☒UNCLASSIFIED/UNLIMITED ☐ SAME AS RPT ☐ DTIC USERS	21. ABSTRACT SECURITY CLASSIFICATION Unclassified	
22a. NAME OF RESPONSIBLE INDIVIDUAL Philip A. Durkee	22b TELEPHONE (Include Area Code) 408-646-3465	22c. OFFICE SYMBOL 63De

DD FORM 1473, 84 MAR   83 APR edition may be used until exhausted   SECURITY CLASSIFICATION OF THIS PAGE
All other editions are obsolete

☆ U.S. Government Printing Office 1986—606-24

Block 19 continued.

a substantially greater reflectance in channel 3, the routine explo[
differences in transmissive characteristics between channels 3 and 4 [
identification. The routine was applied to six case studies which [
been analyzed by three independent experts to establish 'ground trut[
Verification of the cloud analysis results, through a comparison to [
subjective analyses, yielded impressive statistics. A success rate
77.9% was obtained with an arguably small data base of 131 undisp[
scenes. However, problems did arise with the identification of [
clouds and the classification of ocean scenes covered by optically t[
cloud.

An Objective Technique For Arctic Cloud Analysis
Using Multispectral AVHRR Satellite Imagery

by

John P. Barron
Lieutenant, United States Navy
B.S., United States Naval Academy, 1981

Submitted in partial fulfillment of the
requirements for the degree of

MASTER OF SCIENCE IN METEOROLOGY AND OCEANOGRAPHY

from the

NAVAL POSTGRADUATE SCHOOL
March 1988

ABSTRACT

An established cloud analysis routine has been modified for use in the Arctic. The separation of clouds from the snow and sea ice backgrounds is accomplished through a multispectral technique which utilizes AVHRR channel 2 (visible), channel 3 (near infrared) and channel 4 (infrared) data. The primary means of cloud identification is based on a derived channel 3 reflectance image. At this wavelength, a significant contrast exists between liquid clouds and the arctic backgrounds, unlike in the standard visible and infrared images. The channel 3 reflectance is obtained by first using the channel 4 emission temperature to estimate the thermal emission component of the total channel 3 radiance. This thermal emission component is subsequently removed from the total radiance, leaving only the solar reflectance component available for analysis. Since many ice clouds do not exhibit a substantially greater reflectance in channel 3, the routine exploits differences in transmissive characteristics between channels 3 and 4 for identification. The routine was applied to six case studies which had been analyzed by three independent experts to establish 'ground truth'. Verification of the cloud analysis results, through a comparison to the subjective analyses, yielded impressive statistics. A success rate of 77.9% was obtained with an arguably small data base of 131 undisputed scenes. However, problems did arise with the identification of ice clouds and the classification of ocean scenes covered by optically thin cloud.

4

TABLE OF CONTENTS

LIST OF TABLES

LIST OF FIGURES

I. INTRODUCTION

A. MILITARY APPLICATIONS OF AUTOMATED CLOUD ANALYSIS IN THE ARCTIC

In an effort to counter a continually increasing and extensive Soviet military presence in the Arctic, recent U.S. Naval policy has dictated a northward extension of its current fleet operating limits. In the future, cold weather naval operations are planned to penetrate progressively further northward and will likely increase in frequency. Fig. 1.1, drafted by the Vice Chief of Naval Operations for Surface Warfare, depicts this gradual extension of operating limits along with the proposed effective dates of fruition. Such a heightened state of interest in this region places greater significance on a thorough understanding of the arctic environment which can play a critical role in the success or failure of many military operations.

Two of the most dynamic and unpredictable arctic air/sea characteristics that could restrict tactics are the migration of the ice edge and the extent of cloud coverage in the marginal ice zone (MIZ). Naval operations that may be affected by these two variables include surface, subsurface and air operations. Certainly an accurate depiction of the ice edge extent and the total areal coverage of sea ice is necessary for the safe navigation of surface ships and submarines. Similarly, the degree of cloud cover which governs ceilings and visibilities influences tactical carrier air operations supporting anti-submarine warfare, intelligence/reconnaissance, weapons delivery and search and rescue missions among others. Also of great concern is aircraft, flight deck and superstructure icing. According to Naval Air Training and Operational Procedures Standardization (NATOPS) manuals, such icing is a distinct possibility while operating in conditions of less than 4°C in the presence of visible moisture due to clouds or fog.

Since it is evident that sea ice and clouds will play an active role in the conduct of future military operations in the Arctic, it is essential that they be analyzed and forecasted correctly and with the greatest possible degree of accuracy. Recent developments in automated weather analysis systems have made it possible for operational commanders to become more aware of the environment in which they are operating. Automated systems such as the U.S. Navy's Tactical Environmental Support System (TESS) in conjunction with facsimile broadcasts from Oceanography Centers, and the U.S. Air Force's Real-Time Nephanalysis model (RTNEPH), are
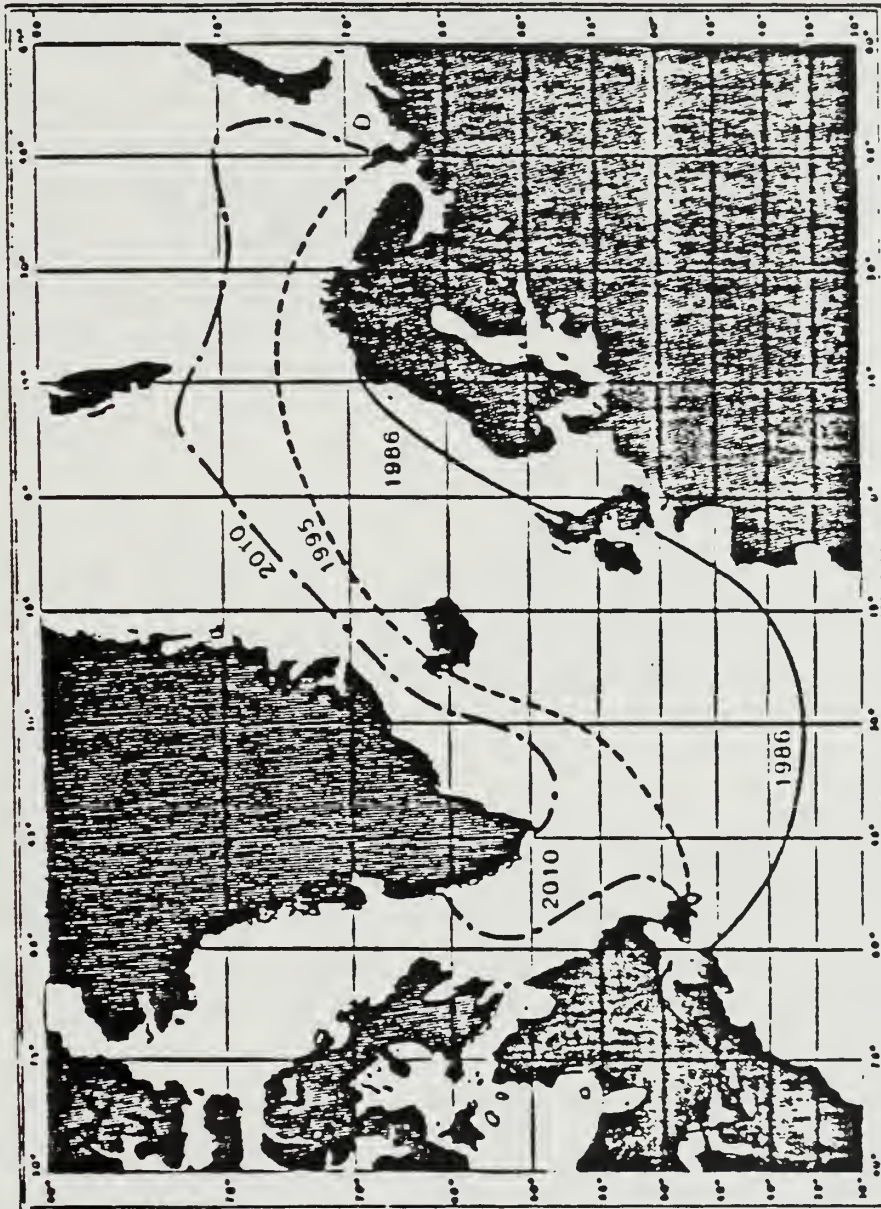
Fig. 1.1   U.S. Navy objectives in northern latitudes.
Severe winter weather limits for the North Atlantic Ocean area.

11

capable of providing deployed military units with quick and easy access to both current analyses and forecasts of environmental conditions.

B.   THE PROBLEM OF SNOW AND SEA ICE/CLOUD DISCRIMINATION

Current satellite data for the RTNEPH automated cloud analysis model originate primarily from the Defense Meteorological Satellite Program (DMSP) spacecraft sensor known as the Operational Linescan System (OLS). The OLS utilizes spectral bands in the infrared (IR) between 10 and 13 μm and in the visible/near infrared (VIS/NIR) between 0.5 and 1.0 μm. An alternate source of satellite cloud data is the Advanced Very High Resolution Radiometer (AVHRR) onboard the National Oceanic and Atmospheric Agency (NOAA) polar-orbiting spacecraft. This sensor samples at five different wavelengths which correspond to the channels listed below:

1.   Channel 1:   0.58 - 0.68 μm (VIS).
2.   Channel 2: 0.725 - 1.10 μm (VIS/NIR).
3.   Channel 3:   3.55 - 3.93 μm (NIR).
4.   Channel 4: 10.30 - 11.30 μm (IR).
5.   Channel 5: 11.50 - 12.50 μm (IR).

As indicated above, the AVHRR sensor, like the OLS, utilizes the IR and VIS/NIR portions of the electromagnetic spectrum. While the use of these wavelengths has been highly successful in mapping cloud cover over most of the globe, weaknesses exist in the polar regions (Raschke et al., 1987).

The ability to distinguish clouds over snow and sea ice backgrounds is greatly degraded when employing the techniques that work well in the lower latitudes. Clouds, snow and sea ice all exhibit similar radiometric properties in both the VIS/NIR and IR spectral regions. In the VIS/NIR, the albedos are similar, while in the IR, it is the thermal signatures that are comparable. These conditions are illustrated in Figs. 1.2 and 1.3, respectively. Fig. 1.2 is an AVHRR channel 2 image of a case study that will be examined more thoroughly in the discussion of the results. To the trained eye, an isolated cloud can be detected over the sea ice, near the center of the image. Objectively, however, the reflectances of the cloud and the background ice are hard to separate. This lack of contrast is even more dramatic in Fig. 1.3, an AVHRR channel 4 image of the same case study. In this scene, the cloud exhibits an emission temperature which is almost identical to that of the sea ice background. Consequently, the overlying cloud becomes nearly invisible. Because the contrast between clouds and snow and ice cover is rather poor at these wavelengths, objective cloud analysis through standard image interpretation routines becomes a rather difficult problem.

Fig. 1.2 Case study: AVHRR channel 2 (VIS/NIR).

Fig. 1.3 Case study: AVHRR channel 4 (IR).

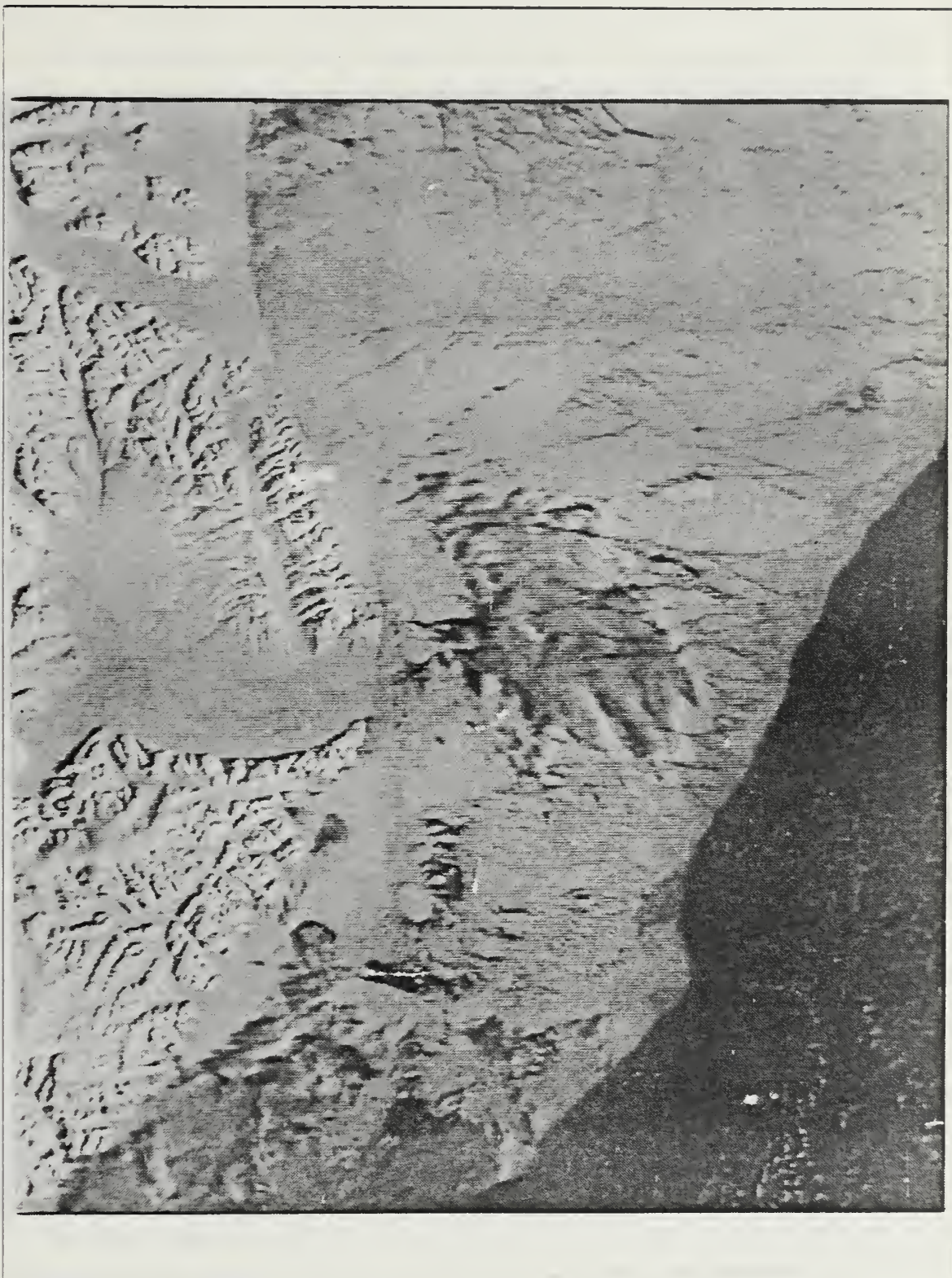As described by Felde *et al.* (1986), the problem of discriminating snow and sea ice from clouds adversely affects the RTNEPH cloud estimations. The VIS/NIR data processor does not even attempt cloud amount calculations over areas where snow or ice cover is believed to exist. The remaining IR data processor handles the cloud analysis in the polar regions, but not without major sources of error. Its ability to detect clouds depends on a comparison between a satellite observed temperature and reference temperatures consisting of a surface background temperature and an atmospheric temperature height profile. Some errors arise from poor estimates of reference temperatures. Other errors arise from atmospheric temperature inversions which are quite common in the Arctic. Since the model assumes that clouds are colder than their background and that the coldest cloud temperatures are associated with the greatest cloud heights, under-estimation or non-detection occurs when the situation is reversed (cloud top temperatures exceeding their background temperatures). This happens frequently in the Arctic when low stratus clouds overlay the snow pack or sea ice. This inadequacy of the automated routine has justifiably spawned several attempts to solve the problem of accurate cloud analysis in the snow and ice environments.

Allen (1987) directed his thesis work toward a multispectral technique capable of discriminating snow from liquid clouds. His approach was based on the works of Bunting and d'Entremont (1982) and Kidder and Wu (1984) who showed that it was possible to use the unique reflectance characteristics in strictly the near infrared portion of the spectrum to discriminate clouds from snow and ice. Bunting and d'Entremont concentrated their work at the 1.6 μm atmospheric window while Kidder and Wu explored the window at 3.7 μm. A sharp contrast between clouds and snow/ice was found to exist at both of these wavelengths. The water droplets of liquid clouds exhibit significant reflectance at 1.6 and 3.7 μm, while the ice particles that make up snow, sea ice and ice clouds yield much lower reflectance values due to their high absorption in the NIR. This is illustrated nicely in Fig. 1.4, an AVHRR channel 3 (3.7 μm) reflectance image of the same case study pictured in Figs. 1.2 and 1.3. In this scene, the isolated cloud that blended in with the sea ice background in channels 2 and 4 stands out noticeably in channel 3.

Allen's technique involved determining the 3.7 μm solar reflectance by subtracting the thermal emission contribution from the total channel 3 radiance measurement. This thermal component was approximated by the AVHRR channel 4 radiance at 11.0 μm. The derived channel 3 reflectance was then used in conjunction
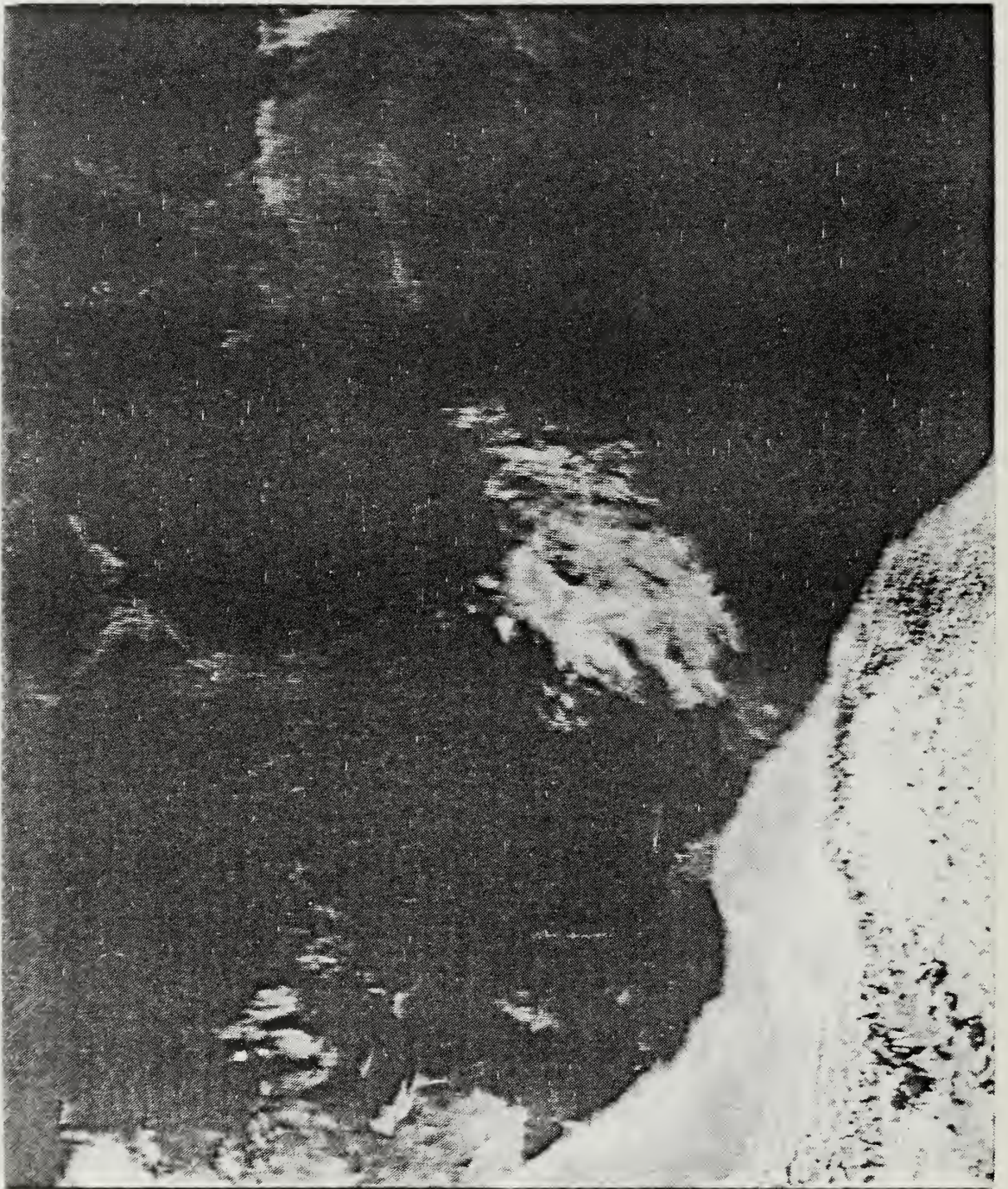
Fig. 1.4   Case study: AVHRR channel 3 reflectance (NIR at 3.7 μm).

16

with VIS and IR radiance values as the basis for a multispectral automated cloud analysis routine that could help solve the problem of snow/cloud discrimination. Allen applied his algorithm to the snow covered areas of the northern continental United States, and for the most part he was quite successful.

This thesis pursues the work of Allen and applies his basic routine, with some modifications, to the unique arctic environment in the quest for better snow and sea ice/cloud discrimination. Chapter II presents the essential radiative transfer theory that is applied in the derivation of the 3.7 μm reflectance and the cloud classification algorithm. In addition, the factors that make cloud analysis in the polar regions such a difficult task are addressed. Chapter III describes the cloud analysis algorithm. The specific modifications incorporated into Allen's routine, which include slightly different classification thresholds and an iterative approach to determining a specific anisotropic reflectance factor, are addressed. The satellite data processing technique is also discussed. In Chapter IV, the data base is introduced. Additionally, the methods of data analysis and verification are presented. The algorithm is then applied to six unique case studies, and the results are presented. Finally, an overall statistical comparison of the experimental results to 'ground truth' is made. Chapter V comments on the effectiveness of the arctic cloud analysis routine, draws pertinent conclusions and suggests recommendations for possible future studies in this endeavor.

II. THEORY

A.   SPECIAL CONSIDERATIONS FOR THE ARCTIC

The unique arctic environment presents many difficulties with standard weather analysis techniques. The use of satellite observations is absolutely critical due to the dearth of synoptic weather observation stations. The shortage of conventional observations is so severe that, often, they can not be used to augment the satellite coverage. This lack of 'ground truth' creates problems for many of the new satellite derived meteorological analysis models that require verification of results. Even the 'last resort' option of referring to climatological data is ineffective since such data bases for the polar regions are scant and unreliable. The cloud/snow and ice discrimination routine developed in this thesis falls prey to this problem of verification.

For the analysis routines that do make use of the satellite data, other problems arise. Continuous polar coverage is not possible since operational imaging is currently available from the two NOAA polar-orbiting spacecraft which are limited to a select number of passes per day. From the data that is usable, Raschke (1987) discusses some obstacles encountered, including:

1. Low radiances. The polar surfaces and troposphere are characterized by the lowest surface temperatures and solar illuminations on earth. This forces current satellite radiometers to operate near one limit of their performance range. This results in less reliable calibration at the lower ends of the brightness scales for solar reflectance (due to the low sun elevation and high solar zenith angles) and thermal emission (due to the low temperatures). The low radiances actually magnify the effects of instrument noise, calibration uncertainties and digitization on these radiance measurements. Noise, in the form of interference patterns due to digitization, has plagued channel 3 (3.7 μm) of the AVHRR since its inception, and is especially evident at the higher latitudes. An example of this noise can be detected in the upper right corner of Fig. 1.4, where light shades in vertical bands are visible against the dark background. The lower radiances also reduce the sensitivity of the measurements to variations in atmospheric, surface and cloud optical properties. Since the discrimination between clouds and clear scenes requires detection of small radiance differences, this lower radiometer sensitivity reduces the overall sensitivity of the cloud analysis itself.

2. Low radiance contrasts. Clouds typically show lower contrasts in solar reflectance over snow and ice surfaces in the VIS and NIR. Contrast reductions in solar reflectance at this portion of the spectrum arise in conditions of

'blazing' snow and arctic haze. The weak polar temperature lapse rates reduce the IR radiance contrasts as well, and inversions may even reverse them. Thus, while the polar conditions demand a more sensitive radiance analysis for cloud separation, the sensitivity in the measurements is reduced by these same conditions.

3. Complex surface variations. Rapid small-scale and larger scale variations in surface properties, particularly reflectance, are often encountered in the marginal ice zone (MIZ) where the movement and redistribution of snow and sea ice takes place within short time intervals. This complicates the usual spatially and temporally constant cloud free scenes which form the basis of many cloud analysis techniques.

4. Non-monotonic relations between radiances and cloud properties. The difference in angular variations of reflected sunlight between rough arctic surfaces and broken clouds, along with the common occurrences of strong temperature inversions, produce non-monotonic variations of radiances with cloud properties, in contrast to the lower latitudes. This renders simple radiance-difference cloud discrimination techniques almost useless due to the actual multi-valued nature of the problem.

Some of the more obvious arctic characteristics that are not addressed by Raschke (1987) include the effect of extended darkness, the degree of atmospheric attenuation and the nature of cloud cover. A cloud analysis routine that makes use of the solar reflectance is, by its nature, restricted to 'daytime' imagery. In the polar regions, the variations in sun elevation essentially create six-month periods of night and day. Obviously, a technique based on solar reflectance measurements is of little worth during the extended winter darkness. The low solar elevations which result in high solar zenith angles also have an effect on atmospheric attenuation and influence the satellite measured radiances. While it is true that a great deal of attenuation is avoided due to the generally low water vapor content of the arctic atmosphere, the effect of the large solar zenith angles acts to increase the attenuation in another fashion. The incoming solar beam simply must pass through more of the atmosphere (at a slant range) at higher values of solar zenith angle, which increases the likelihood of absorption by aerosols and water vapor. Further difficulties arise with cloud/snow and sea ice discrimination from the nature of arctic clouds themselves. A basic assumption of the cloud analysis algorithm tested in this study, is that all liquid clouds are optically thick. However, according to Raschke et al. (1987), the cloud layers over the polar regions are optically thinner than at lower latitudes. Therefore, such an assumption becomes less valid in the Arctic.

B.   THE PRINCIPLES OF RADIATIVE TRANSFER

1. The Equation for Total Radiance

The satellite data base for this thesis is comprised of three of the five AVHRR channels listed in Chapter I. Channel 2 centered at 0.87 μm in the VIS/NIR spectral band, channel 3 centered at the 3.7 μm window of the NIR and channel 4 from the IR spectral region centered at 11.0 μm are the wavelengths utilized. This necessitates a discussion of the radiative transfer characteristics in these portions of the electromagnetic spectrum in order to fully appreciate the basis for the arctic cloud analysis routine.

In the NIR, at the 3.7 μm window, the total radiance measureable at the satellite sensor is comprised of a solar reflectance contribution and a thermal emission contribution. This rather simplified version of radiative transfer is expressed in the following relationship:

$$R = \varepsilon B(T) + r(\theta_o, \theta, \varphi) I \cos\theta_o. \tag{2.1}$$

The term on the left hand side (R) represents the observed radiance at the satellite sensor, while the first term on the right hand side represents the thermal emission contribution and the second term on the right hand side represents the solar reflection contribution. The thermal emission term is defined by the product of the emissivity (ε) and the Planck function (B(T)). The solar reflectance term is a function of the normalized incident solar radiation ($I \cos\theta_o$) and the reflectance of the viewed surface ($r(\theta_o, \theta, \varphi)$).

The validity of this equation is contingent upon three key assumptions. First, any loss of radiance between the satellite sensor and the viewed scene due to atmospheric transmission is considered negligible. Such a restriction is not unreasonable for the polar regions since the amount of water vapor in the atmosphere (the constituent most responsible for attenuation in the NIR) is rather minimal at these latitudes. Secondly, all clouds are considered to be optically thick. This is not very reasonable when considering thin cirrus clouds which will be addressed later in this chapter. Finally, it is convenient to ignore the transmission of these optically thick clouds as well as the snow, sea ice and ocean surfaces as suggested by Bunting (personal communication, 1986). This is substantiated by Hunt (1972) whose theoretical study on the radiative properties of clouds reported essentially zero

transmissivity for optically thick liquid and ice clouds at 3.5 and 11.0 μm. Such an assumption is necessary for the channel 3 reflectance calculation and will be discussed in the description of the cloud analysis algorithm.

At the VIS/NIR wavelength of 0.87 μm, the first term of Eq. 2.1 can be neglected since the effects of blackbody emission, as described by the Planck function, are minimal in this region of the spectrum. Thus, the satellite measured radiance is strictly determined by the solar reflectance term. The value of this term depends on the type of reflecting surface, since each surface has its own unique reflectance characteristics. The reflectance is also anisotropic (directionally dependent) and therefore a function of the solar zenith angle (θ_o), the satellite zenith angle (θ) and their relative azimuth (φ). Fig. 2.1, adapted from Taylor and Stowe (1984), depicts this sun-earth-satellite angular relationship. This anisotropic reflectance and its effects are critical to this study and will be discussed in detail later in this section.
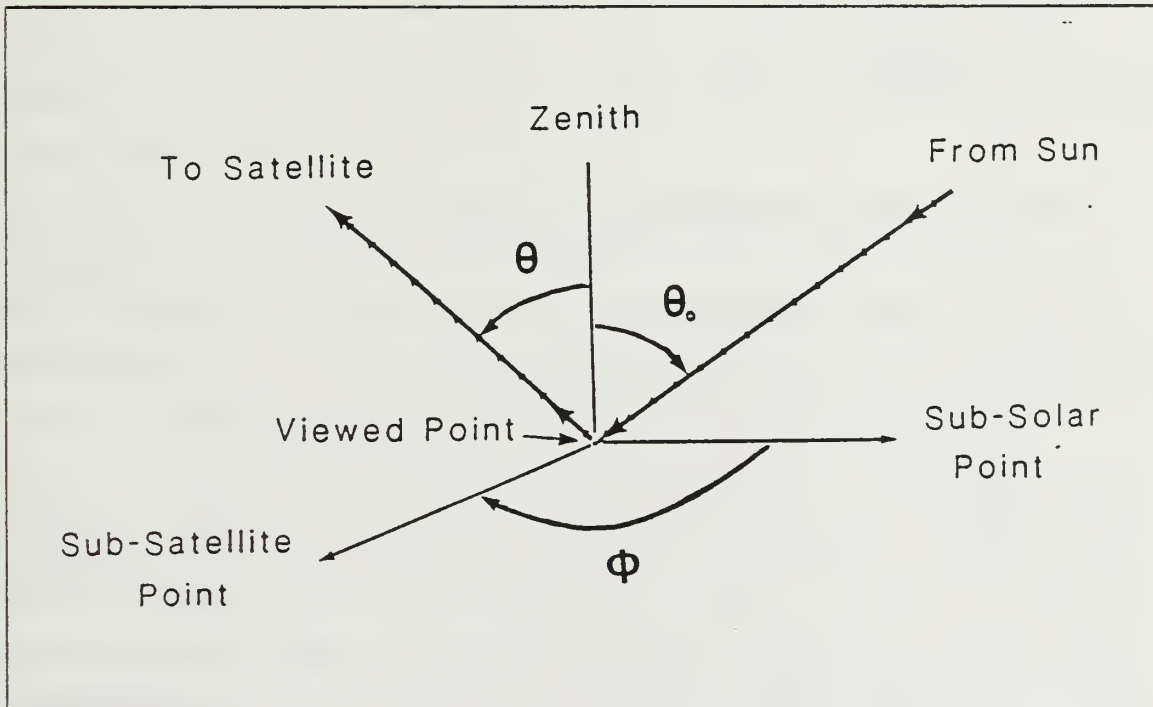

Fig. 2.1   Sun-earth-satellite angular relationship (adapted from Taylor and Stowe, 1984).

In the IR wavelengths at 11.0 μm, Eq. 2.1 can be simplified by neglecting the solar reflectance term. In this portion of the spectrum, the blackbody emission from a surface is near its peak value, thereby rendering any solar reflectance contributions

21

negligible. Consequently, the satellite measured radiance can be accurately approximated strictly by the thermal emission term. The Planck function (B(T)) represents the energy emitted at a particular wavelength and is dependent on the temperature of the radiating surface. The emissivity (ε) is also dependent on the emitting surface and can vary between 0.0 and 1.0. For the purposes of this study however, ε is approximated by 1.0. At 11.0 μm, this assumption is in concurrence with the theoretical findings of Hunt (1972) for optically thick liquid clouds, and Warren and Wiscombe (1980) for both pure snow and snow contaminated by impurities.

2. **The Anisotropic Reflectance Factor**

As mentioned previously, anisotropic reflectance is a function of the solar zenith angle (θ_o), the satellite zenith angle (θ) and the relative azimuth (φ). Taylor and Stowe (1984) define an anisotropic reflectance factor (f) as the ratio between the radiance in a given direction and the radiance that would result if a surface reflected isotropically. This is expressed in the following equation:

$$f = \frac{r(\theta_o,\theta,\varphi)}{r}. \qquad (2.2)$$

Values of f equal to 1.0 correspond to the angles at which an isotropic assumption gives the correct radiant exitance (flux density) for a particular surface. Any departure from 1.0 represents the fractional error that would result if the isotropic assumption was used to estimate total outgoing flux. For example, an f value of 1.5 overestimates the total outgoing flux by 50%, if isotropy is assumed (Taylor and Stowe, 1984).

In general, as θ_o increases, surfaces exhibit more forward scattering and thus higher reflectances. Ignoring this angular dependence of reflectance can result in significant sources of error in the polar regions where relatively high values of θ_o are commonly encountered. Taylor and Stowe (1984) observed reflectances for eight uniform earth and cloud surfaces and illustrated the angular dependence of these reflectances on solar zenith. Ocean surfaces exhibit an increase in reflectance as θ_o increases at all angles. This 'limb brightening' is the result of atmospheric scattering over the relatively dark ocean background. Meanwhile, cloud surfaces appear significantly brighter when viewed from overhead than when viewed from the horizon (greater zenith angles). That is, they experience 'limb darkening' with increasing θ_o. Finally, snow and sea ice reflectances are nearly isotropic, showing very little variation with solar zenith angle.

22

With such varying dependencies on solar zenith angle, particularly at the arctic latitudes, it becomes essential to account for the peculiarities of each reflecting surface. The importance of accounting for the angular dependence of anisotropic reflectance in the Arctic has been confirmed in an experimental study by Grenfell and Perovich (1984). They observed greatly enhanced radiances over snow and sea ice on clear days in the specular reflection direction (high solar zenith angles). They concluded that the anisotropy was large enough to cause significant errors in the calculation of albedo. Ruff and Gruber (1983) illustrated the strong dependence of ocean reflectance on satellite zenith angle. Measurements taken 102 minutes apart for the same geographical location yielded different reflectivities. At a satellite zenith angle near 260°, a reflectivity of approximately 0.04 was measured, while at a satellite zenith angle close to 330°, the measured reflectivity increased to 0.07. Logically, these differences in reflectance were attributed to the varying sun-earth-satellite geometry. The arctic cloud analysis algorithm tested in this thesis accounts for the angular dependence of reflectance by relying on Taylor and Stowe's comprehensive set of tabulated values for f, which is currently the best method available for handling the effects of anisotropy.

C. REFLECTANCES FOR THE ARCTIC SURFACES AND CLOUDS

1. Snow

The albedo of snow is highly variable. According to Foster *et al.* (1987), it is 0.90 or more for freshly fallen snow cover and drops to less than 0.40 if the snow surface is weathered and dirty. The reflectance is dependent on snow parameters such as grain size and shape, impurity content, near surface liquid water content, depth and surface roughness. Other factors including solar zenith angle and cloud cover also contribute to the variability of snow reflectance. At 3.7 μm, ice crystals are highly absorptive which leads to the observed low reflectance for snow. As previously mentioned, the liquid water particles of low clouds are significantly less absorptive (more reflective) at this wavelength. The resulting contrast between the two establishes the basis for this thesis' snow/cloud separation routine.

As snow ages, its reflectance diminishes significantly in the NIR, and to a lesser extent in the VIS/NIR. In the NIR, the albedo may decrease by a factor of two or more whereas at the shorter wavelengths (VIS), reductions in albedo never exceed 10-15% (Wiscombe and Warren, 1980). The greater decrease in reflectivity at longer

wavelengths is largely due to grain size increases caused by melting and refreezing near the surface. These larger grains exhibit higher absorptivity and more forward scattering. The natural addition of atmospheric aerosols and other impurities during the aging process also serves to reduce the snow albedo. The reflectance of snow also decreases as the liquid water content increases. As liquid water replaces the air between the ice grains during the course of melting, the grain size essentially increases since the refractive index of the water is very close to that of ice for wavelengths in the NIR and below. This subsequent increase in grain size serves to reduce the reflectivity of the snow cover, just as it does in the aging process.

Wiscombe and Warren (1980) also addressed the effect of snow layer thickness on albedo. They found that depths less than 1 mm are essentially semi-infinite in the NIR, thereby obliterating the effects of the underlying surface. However, in the VIS NIR, thicknesses up to 20 cm may allow the underlying surface to influence the reflectance. Snow cover over arctic sea ice is often thin enough that its albedo is reduced by the darker ice below.

Wiscombe and Warren (1980) and Foster *et al.* (1987) reported that snow albedo increases at all wavelengths as solar zenith angle increases. This effect is most pronounced in the NIR where it can amount to as much as 0.20 (based on a flat snow surface). This somewhat contradicts the results of Taylor and Stowe (1984), who, as previously mentioned, found very little dependence of snow albedo on solar zenith angle. Cloud cover affects snow albedo by converting direct radiation into diffuse radiation and by altering the spectral distribution of the incoming solar radiation. The conversion into diffuse radiation reduces the effective solar zenith angle and thereby reduces the reflectance.

Wiscombe and Warren (1980) developed a snow reflectance model which accounts for most of the aforementioned factors. Allen (1987) utilized this model to establish his snow reflectance thresholds at 3.7 μm. His values of 0.005 to 0.025 correspond to a semi-infinite snow pack with grain radii between 50 and 200 μm, and solar zenith angles between 40 and 80°. Raschke *et al.* (1987) reported snow reflectances at 3.7 μm to be less than 0.02, and reflectances in the VIS NIR to be greater than 0.55. The separation algorithm which is described in Chapter III, is based on these theoretical limits of snow reflectance.

2. Sea Ice

In a fashion similar to snow, the albedo for sea ice varies extensively. Arking (1987) reported values ranging from 0.20 for sea ice associated with melt ponds, to 0.75 for white sea ice. While this range parallels that of snow, it is generally lower by 10-20%. Taylor and Stowe (1984) hypothesized that the lower sea ice albedo was due to the effects of small unresolved open water areas, greater surface melting and/or shadowing associated with the typically rougher textures of sea ice.

The factors that determine sea ice reflectance are essentially the same as those that determine snow reflectance. The effects of grain size, depth or thickness, near-surface liquid water content, atmospheric impurities, solar zenith and degree of cloud cover all exert the same qualitative influence on sea ice reflectance as they do for snow. However, since sea ice undergoes much less of a change in internal structure with time than snow, the changes in albedo are not as extensive (Arking, 1987).

Two factors which were not previously addressed in the snow section but which significantly affect the reflectance of sea ice include trapped brine and the density of air bubble inclusions. Higher concentrations of brine are found in ice that has not experienced a summer melt season. Similarly, ice that has melted and refrozen displays a greater vapor bubble density (the brine has vacated through percolation) as compared to first year ice. The combined effects of the lower salinity and higher air bubble density make multi-year ice less absorptive and more strongly scattering, which serves to increase its albedo.

This thesis does not differentiate between snow and sea ice reflectances. A multispectral method of discriminating between the two is considered impracticable. Firstly, a great deal of arctic sea ice is actually snow covered. Secondly, the presence of either one creates the same problems with overlying cloud identification. Therefore, the reflectance thresholds established for snow and sea ice are identical.

3. Ocean

Water surfaces display extremely weak solar reflectance in the VIS, VIS NIR and NIR spectral regions (excluding sunglint). This can be related to the previous concept of decreasing reflectivity with increasing particle size. As explained by Bunting and d'Entremont (1982), the oceans are essentially water drops with radii on the order of the radius of the earth. The fact that these bodies of water do not extend to the center of the earth is unimportant, since they are deep enough to absorb all the solar radiance which is not reflected at the surface or by suspended particles.

4. Clouds

The reflectance of clouds is primarily dependent on optical thickness, cloud microstructure, which includes the size and phase (liquid or ice) of the cloud particles, and solar zenith angle. The dependence upon optical depth dominates the other factors at the shorter VIS wavelengths. In the NIR however, Arking and Childs (1985) found the reflectance primarily dependent on the cloud microstructure properties of size and phase. At 3.7 μm, liquid particles are shown to exhibit greater reflectance than ice particles for an entire range of common particle radii (2 to 32 μm). This can be attributed to the higher absorptivity of liquid water at this wavelength. Arking and Childs (1985) also present a more realistic correlation of phase to radius at 3.7 μm. Their typical liquid water cloud particle with a 4 μm radius shows substantially greater reflectance than the typical ice cloud particle of 32 μm. This closely parallels the principle of increasing absorption with increasing grain size discussed previously for snow. The difference in reflectance values exceeds one order of magnitude for an entire range of optical thicknesses between 0.1 and 100.0. Finally, concerning the dependence of cloud reflectance on solar zenith angle, Allen (1987) reported it to be much more appreciable in the NIR than the VIS.

Previous theoretical studies conducted in pursuit of NIR cloud reflectances allowed Allen (1987) to initialize the thresholds for his snow/cloud discrimination routine with a high degree of accuracy. At 3.7 μm, Raschke et al. (1987) identified a minimum liquid cloud reflectance of 0.05 and a maximum ice cloud reflectance of 0.03. Meanwhile, at this same wavelength, Bunting (personal communication, 1986) specified a 0.30 to 0.40 reflectance range for liquid clouds and an approximate reflectance of 0.05 for ice clouds. Allen's own calculations, based on the model of Shettle and Weinman (1970), yielded NIR liquid cloud reflectances between 0.11 and 0.46 for solar zenith angles in the 45-85° range. This thesis takes advantage of Allen's groundwork for the delineation of cloud reflectance thresholds at 3.7 μm. This will be presented along with the description of the cloud separation algorithm in Chapter III.

D. THERMAL EMISSION CHARACTERISTICS OF THE ARCTIC SURFACES AND CLOUDS

The Planck function describes the emitted radiance from a surface as a function of wavelength and the absolute temperature of that surface, in the following fashion:

$$B(\lambda,T) = \frac{2hc^2}{\lambda^5(\exp(hc/\lambda KT) - 1)}. \qquad (2.3)$$

With h, c and K all defined to be constant, it is apparent, for a given wavelength, that the only variable determining the magnitude of the thermally emitted radiance, is the absolute temperature (T in K). Of course, from the discussion of Eq. 2.1, the Planck function is further modified by the emissivity. As alluded to previously, the cloud analysis routine in this thesis approximates ε as 1.0 for all the arctic surfaces. This assumption turns out to be quite valid at 11.0 μm. According to Hall and Martinec (1985), of all the common natural surfaces on earth, water behaves most like a blackbody. Of course, a blackbody is a 'perfect emitter' and is described by an ε equal to 1.0. The emissivity of snow also imitates a blackbody in the IR. Aircraft measurements have recorded a mean emissivity of 0.99 for a melting snow surface (Foster et al., 1987).

As shown in Eq. 2.3, the radiant emission for a fixed wavelength (B(λ,T), is a function of the absolute temperature. In the case of snow and sea ice, the surface temperature, ice crystal size and liquid water content all determine the absolute temperature. Raschke et al. (1987) define the following radiation temperatures for the various arctic surfaces at 11.0 μm:

- ocean   > 270 K.
- sea ice   268 - 270 K.
- snow   240 - 265 K.

Other factors influencing the satellite measured thermal emission include snow depth or sea ice thickness, degree of cloud cover and amount of atmospheric aerosols. The thickness of a snow surface or sea ice cover is only a factor if it is less than a few millimeters deep. This is because the ice crystals display such strong absorption in the IR, thereby making the cover infinitely thick at these small depths. The presence of clouds and aerosols serves to attenuate the upwelled thermal emission from the surface. Although the 11.0 μm region is defined as an atmospheric window, some absorption still takes place (even in the absence of clouds), which causes the satellite measured radiance to be less than the actual surface emission.

Clouds not only interfere with surface induced radiances, but more importantly, contribute their own thermal emission as well. As previously mentioned, the cloud analysis routine in this thesis considers all clouds to be optically thick. Such a stipulation favors the cloud emissivities of 1.0 used in the separation algorithm. However, in reality, a cloud emissivity of 1.0 is only accurate for optically thick liquid clouds. Hunt (1972) calculated the maximum emissivity of cirrus (ice) clouds to be

between 0.50 and 0.70. This is substantially less than his theoretical value of 1.0 for liquid cloud emissivity. As with the earth surfaces, cloud thermal emission is also dependent on absolute temperature. In the IR, this is primarily a function of the cloud-top temperature. In the Arctic, typical IR measured cloud top temperatures range from 245-265 K for liquid clouds, and fall below 255 K for ice clouds (Raschke *et al.*, 1987).

E.   THE PROBLEM OF ICE CLOUDS

The distinctly different reflective properties of liquid and ice particles at 3.7 μm enable liquid clouds to be easily distinguished from the ice backgrounds of the Arctic. However, a problem exists for clouds composed of ice particles. For the most part, the contrast in reflectance between ice clouds and snow/sea ice is not drastic enough to allow for easy separation. Occasionally, some ice clouds demonstrate higher reflectivities than their ice backgrounds. In these cases, the greater reflectance is due to the substantially smaller particle sizes in the upper portions of ice clouds compared to the larger grains in the snow and sea ice cover (Bunting, personal communication, 1986). Unfortunately, most thin cirrus is composed of large ice crystals whose radii are similar in size to snow and ice cover. To deal with this dilemma, Allen (1987) took advantage of differences in transmissive properties of ice clouds between the NIR and IR spectral regions.

The presence of optically thin clouds contributes to differences in satellite measured brightness temperatures between the NIR (AVHRR channel 3) and the IR (AVHRR channel 4). In theory, neglecting any solar reflectance, this is the result of two contributing factors. Firstly, thermal emission as a function of temperature varies with wavelength. Secondly, the transmissivity of optically thin clouds is dependent upon wavelength. At 3.7 μm, the surface thermal emission dominates any cloud emission, while at 11.0 μm, the relative thermal radiation from within the cloud is much greater. At the same time, the transmission of surface radiance through the cloud is enhanced at the shorter wavelengths. These effects combine to produce brightness temperature differences. In reality however, the effect of solar radiation in the NIR can not be ignored. From the discussion on the equation of total radiance, it is known that solar reflectance contributions are quite evident in the NIR, but essentially negligible in the IR. This also leads to brightness temperature differences at these wavelengths.

28

The differences in observed brightness temperatures between channel 3 and channel 4 are thus a net result of differential solar reflectance effects and differences in cloud transmissivity at these wavelengths. Stephens (1981) related the relative contributions of these two effects with cloud optical depth. At large optical depths (greater than 10.0), brightness temperature differences are strictly a consequence of solar reflectance from the cloud surface. Similarly, at small optical depths (less than 0.1) where transmission through the cloud is readily accomplished, solar reflectance from the earth's surface is the primary factor responsible for the brightness temperature differences. Only within a rather restricted mid-range of optical depths (0.5 to 2.0) does the effect of cloud transmissivity overcome solar reflection as the primary contributing factor to differences in channel 3-channel 4 brightness temperatures.

As illustrated by Allen (1987), the distinction between cirrus and snow/sea ice is accomplished in the region where the effects of transmissivity differences are larger than the effects of solar reflectance. To discriminate ice clouds from snow, Allen derived (after Stephens, 1981) a unitless factor (F_t) which accounts for these transmissivity induced differences in brightness temperature between channel 3 and channel 4. This factor, proportional to the ratio of channel 4 to channel 3 brightness temperatures, is expressed in the following equation:

$$F_t = \frac{T_4}{T_3 - T_4}. \tag{2.4}$$

For clear sky cases, where the temperature difference between channel 3 and channel 4 is minimal, the factor is large. Likewise, for cases with optically thin ice clouds, where the transmissivity creates a difference in brightness temperatures, the factor becomes noticeably smaller. The cloud analysis algorithm establishes a critical threshold for F_t which ultimately determines the presence or absence of thin cirrus clouds. This will be addressed in the algorithm development section.

III. THE ALGORITHM

A.   PROCESSING AVHRR DATA

The method of converting raw satellite data into reflectances and brightness temperatures follows that of Allen (1987). The following sections address the derivation of the channel 2 reflectance, the channel 3 reflectance, the channel 3 brightness temperature and the channel 4 brightness temperature. Thresholds based on all of these parameters are the crux of the cloud analysis algorithm.

1. Channel 2

The channel 2 data are calibrated in terms of albedo (Lauritson et al., 1979). This albedo is weighted by the cosine of the solar zenith angle to account for its directional dependence. It is further scaled in a range of gray shade values from 0 to 255 by simply dividing by a constant. The resultant channel 2 reflectance is utilized as a threshold for the classification of ocean scenes. Channel 2 reflectance thresholds are not used to discriminate clouds from the snow and sea ice due to the insufficient contrast between these scenes at this wavelength.

2. Channel 3

The channel 3 data are calibrated in terms of radiances (Lauritson et al., 1979). These radiances include contributions from solar reflectance and thermal emission. According to Allen (1987), the radiance from liquid clouds is composed primarily of solar reflectance, while the radiance from the less reflective earth surfaces and ice clouds is composed of nearly equal amounts of solar reflectance and thermal emission. As previously mentioned, the extraction of the channel 3 solar reflectance from the total channel 3 radiance measurement is the essence of the cloud separation routine tested in this thesis.

The following procedures which outline the separation of the solar reflectance from the thermal contribution at 3.7 μm, were initially suggested by Bunting (personal communication, 1986) and later performed by Allen (1987). Applying the basic radiative transfer relationship described by Eq. 2.1 to channel 3 yields:

$$R_3 = \varepsilon_3 B_3(T) + r_3(\theta_o, \theta, \varphi) I_3 \cos\theta_o. \tag{3.1}$$

Now, ignoring the transmission of both the earth surfaces and clouds (recall that all clouds are assumed to be optically thick), and assuming for now, isotropic radiation, emissivity can be expressed in the following fashion:

$$\varepsilon_3 = 1 - r_3. \tag{3.2}$$

Now, considering the anisotropic reflectance factor discussed in Chapter II, Eq. 3.2 can be rewritten as:

$$\varepsilon_3 = 1 - \frac{r_3(\theta_o,\theta,\varphi)}{f}. \tag{3.3}$$

Substituting Eq. 3.3 into Eq. 3.1 yields:

$$R_3 = (1 - \frac{r_3(\theta_o,\theta,\varphi)}{f})B_3(T) + r_3(\theta_o,\theta,\varphi)I_3\cos\theta_o. \tag{3.4}$$

Finally, solving for channel 3 reflectance gives:

$$r_3(\theta_o,\theta,\varphi) = \frac{R_3 - B_3(T)}{I_3\cos\theta_o - B_3(T)/f}. \tag{3.5}$$

The thermal emission contribution ($B_3(T)$) is closely estimated by solving for $B_4(T)$ in the following equation:

$$B_4(T) = R_4'\varepsilon_4. \tag{3.6}$$

As stated previously, this simplification of Eq. 2.1 in the IR regime is quite valid, and ε_4 is approximated nicely by 1.0. Thus, the thermal component of the channel 3 radiance ($B_3(T)$) is realized directly from the satellite measured radiance of channel 4 (R_4). The normalized incident solar radiance ($I_3\cos\theta_o$) was calculated by Allen (1987) as follows:

- NOAA- 9 = 5.31085 mW/m^2 cm^{-1} sr.
- NOAA-10 = 5.26415 mW/m^2 cm^{-1} sr.

The channel 3 brightness temperature is utilized in discriminating ice clouds from the snow and sea ice backgrounds. It is determined from Eq. 2.3, which related the Planck function to the wavelength and temperature of an emitting surface. Of course, it is necessary to invert the equation to solve for the brightness temperature. The central wavelength of channel 3, which is required for the calculation, applies to a temperature range of 225 to 320 K (Allen, 1987). This likely covers the extent of arctic temperatures during the six-month period of daylight for which this algorithm is designed.

3. Channel 4

The channel 4 data are calibrated to radiances in a fashion similar to channel 3 (Lauritson *et al.*, 1979). At this wavelength, the total radiance is determined strictly from the thermal emission which can be represented by a brightness temperature. However, a correction factor must be applied to the satellite measured radiance prior to conversion into a temperature. The NOAA-9 data undergo a non-linear correction in the form of a polynomial interpolation, while the NOAA-10 data are converted after a linear interpolation correction scheme is employed (Allen, 1987). The channel 4 brightness temperature is found by inverting Eq. 2.3 at the central wavelength of approximately 11.0 μm. As outlined by Lauritson *et al.* (1979), the use of this central wavelength corresponds to temperature range of 225 - 275 K. Consequently, the algorithm sets temperatures less than this range to 225 K and temperatures greater than this range to 275 K. Once again, this range should be sufficient to include the actual arctic temperatures encountered during the six-month summer daylight period.

B.   CLASSIFICATION THRESHOLDS

The primary function of the algorithm is to distinguish cloud cover from the arctic backgrounds. Since there is little difference between the reflective and emissive properties of snow and sea ice, it is an extremely difficult task to accurately separate the two surface types. Therefore, as alluded to in Chapter II, this algorithm makes no distinction between these two arctic surfaces. On account of this, future references to either of these two surfaces in the context of algorithm classification are interchangeable. While the radiative properties of liquid clouds and ice clouds do exhibit certain differences, the overall classification of cloudy versus cloud-free scenes is the ultimate objective. Thus, this algorithm does not differentiate between cloud type, even though the methods of identifying liquid and ice clouds are based on different physical principles.

The critical decision making process of the cloud analysis algorithm is based on a threshold comparison technique. The decision process is essentially a four-step sequence which ultimately classifies each pixel as cloud, ocean or snow.

The first step is the separation of liquid clouds from the arctic earth surfaces which is easily accomplished by evaluating the differences in channel 3 reflectance. Liquid cloud reflectance values at 3.7 μm are substantially greater than the values observed for ocean, snow and sea ice. In Chapter II, various theoretical ranges for liquid cloud reflectance in the NIR were presented. The lowest reported limit of 0.05, documented by Raschke *et al.* (1987), is used to define this algorithm's critical classification threshold for liquid clouds. Since this value is well separated from the theoretical values for the other arctic surfaces, all pixels exhibiting a channel 3 reflectance greater than or equal to 0.05 are consequently identified as cloud.

The second step in the decision process isolates the ocean scenes from the snow and ice. The most effective means of executing this involves a comparison of the channel 2 reflectances. As addressed in Chapter II, the theoretical reflectance of water surfaces is quite small at all wavelengths. The contrast between ocean and snow is most pronounced in channel 2. Raschke *et al.* (1987) defines channel 2 reflectance values for ocean surfaces to be less than 0.07, while the values for snow and sea ice are both greater than 0.55. The value of ocean reflectance is actually smallest in channel 3, where it never exceeds 0.02. However, snow and sea ice maximums are equally as small at this wavelength. The stark contrast available in channel 2 constitutes the critical threshold for ocean scene classification. A maximum value of 0.45 is established for this threshold. While at first glance, this appears to be an excessive upper bounds for ocean reflectance, it is necessary in order to reduce the number of ambiguous cases arising from the anisotropic reflectance factor iteration which is described in the next section. The additional stipulation of a channel 3 reflectance maximum of 0.05 also serves to limit the amount of potential ambiguous cases. To summarize, pixels with a channel 2 reflectance less than 0.45 and a channel 3 reflectance less than 0.05 are classified as ocean.

The third step of the classification sequence identifies the snow and sea ice scenes. At this point in the algorithm, the only unclassified scenes are pixels with a channel 2 reflectance greater than or equal to 0.45 and a channel 3 reflectance less than 0.05. According to Raschke *et al.* (1987), snow and sea ice both exhibit channel 2 reflectances greater than 0.55. Allen (1987) found the maximum channel 3 reflectance

of snow to be 0.025. Thus, these theoretical and experimental reflectance ranges for snow and sea ice are completely included within the scenes yet to be classified. This ostensibly guarantees that no snow or sea ice pixels have been isolated by the first two steps of the decision sequence. However, a blanket categorization of the remaining scenes as snow is not appropriate. While the channel 3 reflectance of some ice clouds is sufficient to meet the liquid cloud threshold of 0.05, it is likely that most of the ice clouds escaped detection in step one.

To distinguish between the heretofore unclassified ice clouds and the snow and ice background, the temperature factor (F_t) introduced in Chapter II is employed. After much experimentation, Allen (1987) found that an F_t less than 15.0 was the most efficient in identifying the majority of the optically thin cirrus that had not been classified by their channel 3 reflectance. This algorithm takes advantage of Allen's groundwork by similarly setting the temperature factor threshold to 15.0. In short, the third step of the decision process defines snow and sea ice scenes as pixels whose F_t is greater than or equal to 15.0.

The fourth step of the algorithm defines all the pixels yet to be classified as cloud. This ensures that all scenes have been categorized as either ocean, snow or cloud. The most likely candidates that have eluded classification up until this point are optically thick ice clouds whose transmissivity precluded the requisite channel 3 and channel 4 brightness temperature differences from being exploited by the temperature factor. Table 1 summarizes the four-step decision making process of the algorithm tested in this thesis, while Table 2 highlights the classification thresholds utilized in Allen's routine.

Due to the nature of the algorithm, a fourth classification category is possible. An ambiguous category, based on the certainty of the particular anisotropic reflectance factor utilized, is possible besides the aforementioned ocean, snow and cloud options. This ambiguous classification is addressed in the following section.

C.   CONSIDERATION OF ANISOTROPIC REFLECTANCE

In Chapter II, the importance of the anisotropic reflectance factor (f) was highlighted. According to Taylor and Stowe (1984), the effects of anisotropy are most evident at large solar zenith angles, large satellite zenith angles and large relative azimuths. Allen (1987) verified this with his comparison of isotropic reflectances and reflectances modified by the anisotropic reflectance factor. In particular, he found that scenes in which the satellite sensor was viewing in the direction of the sun, and scenes

TABLE 1

THE FOUR-STEP CLASSIFICATION PROCESS

	Scene type	Threshold
1.	Liquid cloud	CH 3 REFL > 0.05
2.	Ocean	CH 3 REFL < 0.05 and CH 2 REFL < 0.45
3.	Snow/Sea Ice	F_t > 15.0
4.	Ice cloud	otherwise

TABLE 2

THE CLASSIFICATION THRESHOLDS OF ALLEN

	Scene type	Threshold
1.	Liquid cloud	CH 3 REFL > 0.057 and CH 1 REFL > 0.19
2.	Land	CH 1 REFL < 0.19
3.	Snow	F_t > 15.0
4.	Ice cloud	F_t < 15.0

in the vicinity of the satellite subpoint at large solar zenith angles experienced the greatest deviations in reflectance when anisotropy was neglected. In the Arctic, these two conditions are typical, and therefore, accounting for anisotropy becomes critical for accurate reflectance calculations.

The algorithm employed in this thesis is a refinement of Allen's technique, and in fact, it was initially proposed by him as a recommendation for improvement. His routine used an average value of f (adapted from Taylor and Stowe, (1984)) for the

surfaces likely to be encountered. These included land, snow and liquid cloud. However, since the choice of the anisotropic reflectance factor can ultimately determine the scene classification, it was thought to be too important to neglect the variations in f among the unique reflecting surface categories, as Allen did. Thus, the use of Taylor and Stowe's (1984) tabulated values specific to each arctic surface is utilized in this algorithm. These include ocean, snow, low cloud and high ice cloud.

As suggested by Allen (1987), a preliminary scene classification is made based on an average value of the anisotropic reflectance factor calculated from the aforementioned arctic surfaces. An iterative process is then employed to determine the correct factor for the particular classification. The exact procedure is outlined as follows:

1. The average value of f is determined from the ocean, snow, liquid cloud and ice cloud tables specified in Taylor and Stowe (1984) for the specific solar zenith angle, satellite zenith angle and relative azimuth.

2. The algorithm makes an initial scene classification with this average f based on the threshold technique previously described.

3. The routine repeats the classification process using the anisotropic reflectance value particular to the classification category just determined, and reclassifies.

4. If the reclassification is the same as the initial classification, the scene is accepted as that particular surface.

5. If the reclassification does not match the initial classification, the process is repeated using the value of f corresponding to the most recent classification.

6. This process is further repeated until two successive classifications are identical, in which case the scene is subsequently accepted as that particular surface.

7. If the iteration is repeated five times without two successive classifications matching, the scene is categorized as ambiguous.

The inclusion of an ambiguous category adds a greater degree of certainty to the other classifications of snow/sea ice, ocean and clouds. At the same time, the identification of ambiguous pixels is designed to detect two possible types of scenes. The first is a pixel that represents a transition between two different surface types. The second is a pixel whose field of view (FOV) is simultaneously composed of more than one type of reflecting surface. Essentially, both cases represent 'mixed' FOV scenes, in that the pixel area is comprised of two or more different reflecting surfaces. In a 'mixed' FOV scene, both the combination of differing reflectance characteristics and the percentage of total areal coverage by each surface, affect the ultimate scene classification. The presence of thin clouds overlying the arctic surfaces is an example of such a 'mixed' FOV scene.

The ability of a cloud analysis algorithm to detect thin clouds is of obvious importance. The identification of thin clouds over the ocean surface is thought to be possible with this algorithm. Since the anisotropic reflectance factor values for the ocean are the most unique, and differ significantly from the other surfaces, the likelihood of not matching two successive classifications is the greatest for this type of scene. Thus, detection of thin clouds which have avoided identification by the standard threshold techniques, may be possible through further evaluation of the ambiguous scenes. This will be investigated in the next chapter as the algorithm is applied to real data.

IV. RESULTS

A.   DATA

As a measure of performance, the arctic cloud analysis routine was applied to satellite data collected during the recent Marginal Ice Zone Experiment (MIZEX 87) conducted in the East Greenland Sea during March and April of 1987. Satellite coverage was provided by the two polar-orbiting NOAA spacecraft (NOAA-9 and NOAA-10). Between March 22 and April 10, three passes per day were available for analysis. These included an eight-minute pass from NOAA-9 in the early morning, a late morning, eight-minute NOAA-10 pass and a four-minute pass from NOAA-10 during the late afternoon. An initial screening of 244 minutes of AVHRR data in channel 2 subjectively narrowed this extensive data base down to six four-minute passes (overviews) to be used in the evaluation of the analysis routine. While the algorithm is capable of processing both NOAA-9 and NOAA-10 data, the six overviews chosen were all derived from the late morning NOAA-10 passes. The quality of these images in terms of darkness/brightness was generally much better than the early morning and late afternoon orbits. Additionally, the extent and location of the swath was more appropriate in that known geographical landmarks were easily identifiable for reference and familiarization. Finally, the overviews chosen exhibited a nearly equal temporal spacing in covering almost the entire span of the satellite coverage, thereby adding increased independence to the statistical verification scheme which will be introduced in the next section.

A 512 x 512 pixel subscene was chosen from each of the six overviews to test the algorithm performance. The criteria for selecting the subscenes were simply a requisite presence of snow or sea ice, ocean and liquid cloud in nearly equal proportions. The extent of cirrus (ice) clouds also weighed favorably in a number of cases. By these standards, an ideal subscene was one in which the sea ice or snow covered land was adjacent to the open ocean, and the sky cover was either broken or scattered by both high and low clouds. The locations of the six subscenes chosen as case studies are illustrated in Fig. 4.1 and correspond to the following times of initial satellite overpass (all times local):

- Case 1   1119, 06 April 1987.
- Case 2   1004, 05 April 1987.

- Case 3   1048, 03 April 1987.
- Case 4   0947, 01 April 1987.
- Case 5   1000, 27 March 1987.
- Case 6   1042, 25 March 1987.

B.   METHOD OF VERIFICATION

1. Subjective Analysis

The true value of a cloud analysis algorithm only can be determined after a comparison with confirmed cloud conditions. In the case of the Arctic, conventional surface cloud cover observations and aircraft pilot reports (PIREPS) are simply not extensive enough to provide an objective and accurate account of the actual cloud conditions. The most common alternative in such a data sparse region is to rely on subjective satellite analysis for the 'ground truth'. Qualified analysts can distinguish cloud cover over arctic backgrounds by several methods. Textural features, orography, the time evolution of images and the overall synoptic picture can all be used by an analyst to identify the extent of cloud cover. In the Arctic, features such as colder cloud tops, cloud shadows on the snow and ice, illumination of cloud sides and cracks and leads in the sea ice usually facilitate cloud recognition (Ebert, 1987).

However, manual subjective satellite cloud analysis is not without its drawbacks. By its very nature, subjective analysis is not consistent, in that no two analysts will interpret an image in precisely the same fashion. Similarly, repeatability by an individual analyst or a group of analysts is never assured. The accuracy of the analysis is also limited by the quality and resolution of the reproduced image displayed on either paper or a monitor. Finally, manual analysis is a slow process that can be extremely time consuming if many images require interpretation. Of course, this is a primary reason behind the development of automated cloud analysis routines.

The subjective analyses of three independent experts were used to assess the performance of the cloud analysis routine developed in this thesis. In the following section, the technique employed by these analysts to verify the results of the algorithm is described in detail.

2. The Analysts' Technique

All three analysts were provided with a 5.0 x 6.5 inch, channel 2 overview along with three separate 6.5 x 6.5 inch subscene images for each of the six case studies. The subscene images included a channel 2 reflectance image, a derived channel 3 reflectance image and a channel 4 brightness temperature image. Also supplied to
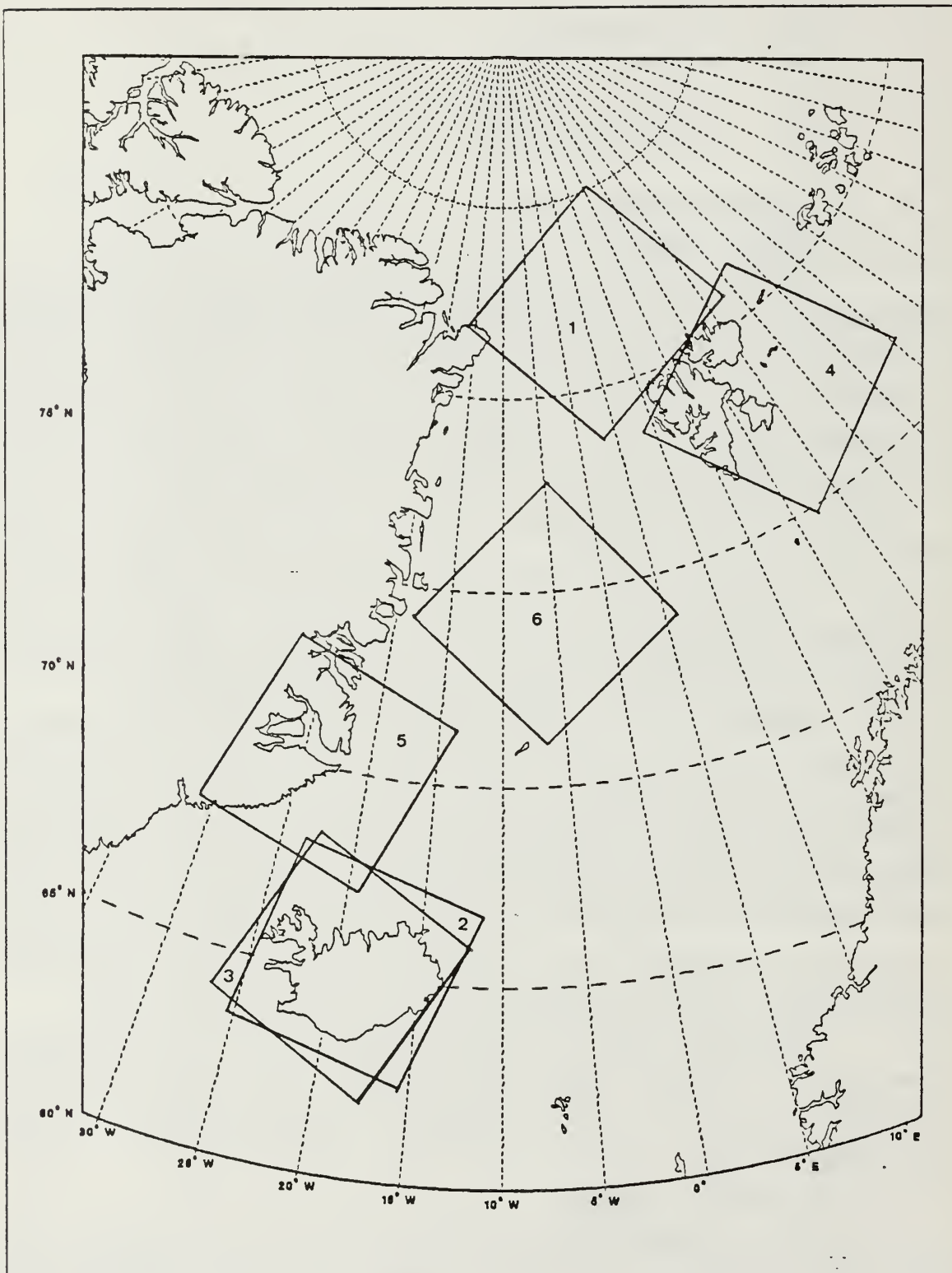
Fig. 4.1   Subscene locations.

each analyst were three 6.5 x 6.5 inch acetate grids with 36 points divided into six rows and six columns, separated by 1.0 inch. The analysts were tasked to overlay a grid onto each subscene image per case study and to classify the scene underneath each point. The use of the three grids and three channels served only as an aid for classification. It was only necessary to classify 36 points for each case study. Thus, a total of 216 points or scenes were classified by each analyst.

The analysts were given the option of using six distinct categories to classify a particular point. These included ocean, snow, sea ice, liquid cloud, ice cloud and a special boundary category. The boundary category was made available to alleviate errors arising from acetate misplacement and to account for the fact that each grid point is actually a small area or FOV, rather than a precise point. Consequently, the analysts were required to identify grid points at a transition between two or more different surface types as boundaries. Along with each boundary classification, the analysts annotated the distinct surface types that existed on each side of the interface. This was done to expand the data base since analysts were not likely to match each classification exactly due to acetate placement. In the case of arctic surfaces visible through overlying optically thin clouds, the analysts identified the scenes as cloud. Finally, as previously mentioned, the algorithm makes no differentiation between snow and sea ice or liquid cloud and ice cloud. However, the analysts were asked to make these distinctions in order to clarify potential problem areas arising from the cloud analysis routine.

3. Results of the Subjective Analysis

Scene classification by the algorithm loses credibility if the scenes can not be accurately classified by the analysts. Since verification by the subjective 'ground truth' is the only way to measure the success of the cloud analysis routine, a high degree of certainty regarding scene classification must first be established by the analysts. Of the total 216 points that were classified, the analysts were in agreement on 131 classifications. This amounts to 60.6%, which represents a significant reduction in the data base. Such variability encountered among the experts, in itself, dramatically underscores the need for an objective routine. The number of scenes that were clearly in dispute among the analysts totaled 33, which equates to 15.3%. These scenes included points in which at least one analyst's classification did not match the other classifications, *and*, in which a boundary classification was not specified by any of the analysts. The other cases of discrepancy involved either one or more boundary

classifications. Of course, the simplistic technique of scene identification by the acetate grid, was likely responsible for the majority of the cases in disagreement.

The 131 cases in exact agreement and the 33 cases in exact disagreement did not include any of the boundary categorizations that were used quite liberally by the analysts. Altogether, 58 scenes, representing 26.9% of the cases, were classified as a boundary by at least one of the analysts. As a means of post-analysis quality assurance, each of the 58 scenes classified as a boundary was subsequently checked to ensure that an actual transition between surface types occurred within a 1.0 mm radius circle encompassing the grid point. Additionally, either one or both of the elements constituting the boundary was required to match the other analysts' choice of classification. Subjecting the boundary scenes to these criteria, narrowed the number of legitimate boundary cases down to 52. The addition of these cases to the number of cases in exact agreement, resulted in a total of 183 scenes available for verification purposes. This equates to an acceptance rate of 84.7%, which noticeably increases the verification data base. While the overall increase in useable grid points adds more credibility to the comparison statistics, at the same time, the criteria for inclusion of the boundary cases may not have been stringent enough to legitimize the statistical results. Thus, an evaluation of both sets of data (cases of exact agreement and cases with boundaries included) is performed. A summary of the subjective analysis statistics is listed in Table 3.

TABLE 3
RESULTS OF THE SUBJECTIVE ANALYSIS

Total points	216	
Clearly disputed points	33	15.3%
Exact agreement	131	60.6%
Boundaries included	183	84.7%

C. RESULTS OF THE CLOUD ANALYSIS

This section addresses the results of the cloud analysis algorithm for each of the six case studies. While this discussion includes a general comparison of the algorithm scene classifications to the classifications by the subjective analysis, the primary focus is on problems encountered, and the features that make each case unique. The results derived from the cloud analysis for each of the six cases are displayed in Figs. 4.3 - 4.8 of this section. These analysis images are color coded according to the category of scene classification. Pixels of open ocean appear dark blue, while snow and sea ice pixels exhibit an aqua color and clouds show up in a light grayish-green. The ambiguous scenes are represented by the red pixels. For a more complete account of the satellite imagery applicable to each case, refer to the Appendix, where the analysis results, the channel 2 reflectance, the channel 3 reflectance and the channel 4 infrared images are all presented.

1. Case 1

Case 1 is a subscene taken from the NOAA-10 overview initiated at 1119 local time on 6 April 1987. The subscene is centered over fast ice located to the north of Spitzbergen. The cloud analysis results for this case are pictured in Fig. 4.2. In the upper left corner of the analysis subscene, a distinct portion of cloud cover extends from the ocean to well beyond the ice edge. This is clearly evident as thin, low cloud in the images from channels 2, 3 and 4. Also apparent in the analysis subscene, is a cloud band crossing the ice edge at the bottom of the image. While not displaying a high reflectance in channels 2 and 3, the same band appears as an obvious streak of cirrus in channel 4, where it exhibits much colder temperatures than the underlying surfaces. It is apparent from this case that the analysis routine is quite capable of identifying both liquid and ice clouds.

It is interesting to note the apparent underestimation of ocean scenes in this case. It appears that the analysis has overestimated the degree of cloud cover at the expense of the ocean pixels. Relatively few ocean pixels are visible in the images of channel 3 reflectance and the cloud analysis, while at the same time, the extent of the ocean pixels appears to be much greater in the conventional VIS and IR images. Since the experimental technique of determining the channel 3 reflectance by extracting the thermal emission contribution from the total radiance measurement involves certain assumptions and approximations, as well as numerous calculations, it is more likely that the images of channels 2 and 4 represent a more accurate portrayal of the true

cloud conditions. The apparent overestimation of liquid cloud in channel 3 is likely due to the fact that the prevalent cloud layer is optically thin. In the case of optically thin liquid clouds, the underlying surfaces are visible in channels 2 and 4, but not in channel 3. This is because even the thinnest liquid clouds exhibit such a great reflectivity in the NIR that the background surfaces are effectively obscured. Since the algorithm identifies clouds primarily by this NIR reflectance in channel 3, the ocean pixels that are apparent in channels 2 and 4, are identified as cloud by the analysis routine. The obscuration of ocean pixels also occurs in the presence of the cirrus band, but to a lesser extent.

Two other points are worthy of note concerning Case 1. The first is the rather minimal number of red pixels. The vast majority of these ambiguous scenes are located at transitions between ocean and either snow or cloud pixels. The second point of note is the existence of noise, which manifests itself as cloud pixels in vertical bands. It is most apparent in the cirrus streak overlying the ice at the bottom of the image. As mentioned previously, this noise is inherent to channel 3 of the AVHRR sensor, and, beyond the control of this cloud analysis routine.

2. Case 2

The subscene depicted in Case 2 is comprised of Iceland and the surrounding ocean. It is part of the NOAA-10 pass that commenced at 1004 local time on 5 April 1987. The results of the analysis for this case are pictured in Fig. 4.3. As with the first case study, both liquid and ice cloud are evident in the images of channels 2, 3 and 4. The thick liquid cloud that dominates the lower left portion of the image, as well as the top and extreme right side, is easily identified in the analysis by its significant channel 3 reflectance. However, the possible overestimation of optically thin liquid cloud that was discussed in the previous case, seems to be in evidence here as well. To the north of Iceland, the extent of cloud cover in channel 3 appears to be much greater than in channel 2, although only slightly greater than in channel 4. Additionally, some of the ice cloud which is visible as a band of cirrus stretching across the lower half of the island, does not meet the channel 3 reflectance threshold. Consequently, much of the cirrus band that is readily apparent in the IR imagery is lost in the overall cloud analysis. Apparently, the temperature factor (F_t), designed to handle this type of ice cloud is not entirely successful.

The number of ambiguous pixels identified in the analysis of this case is appreciable. A significant section to the northeast of Iceland has been classified as
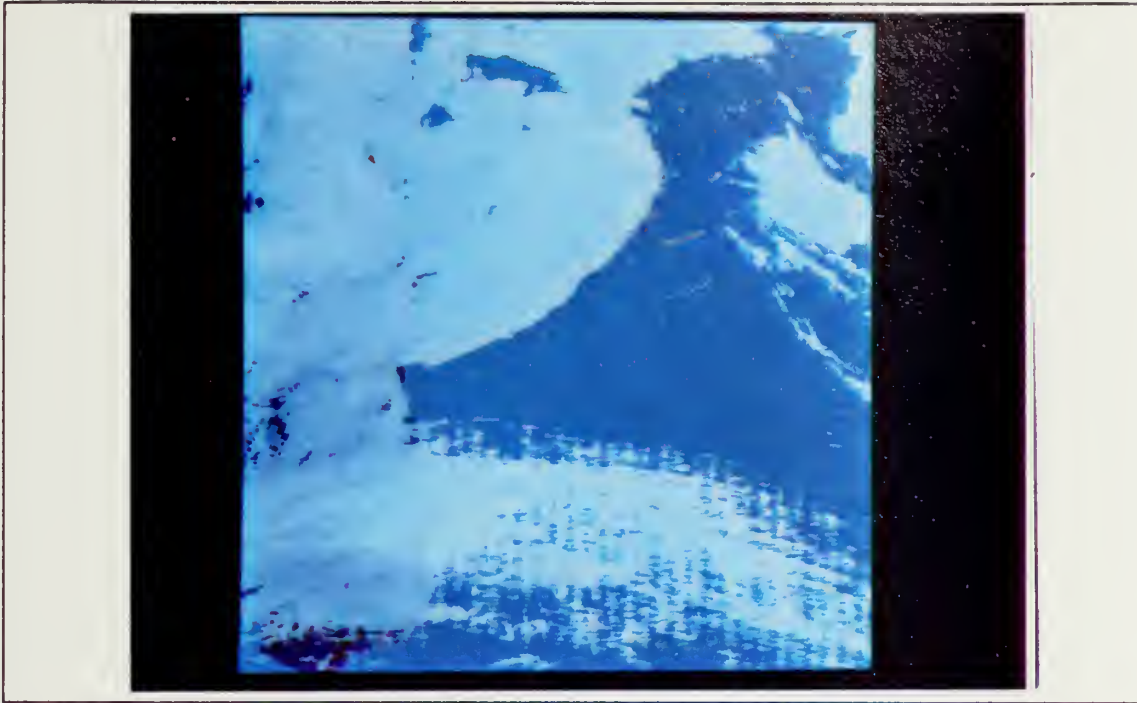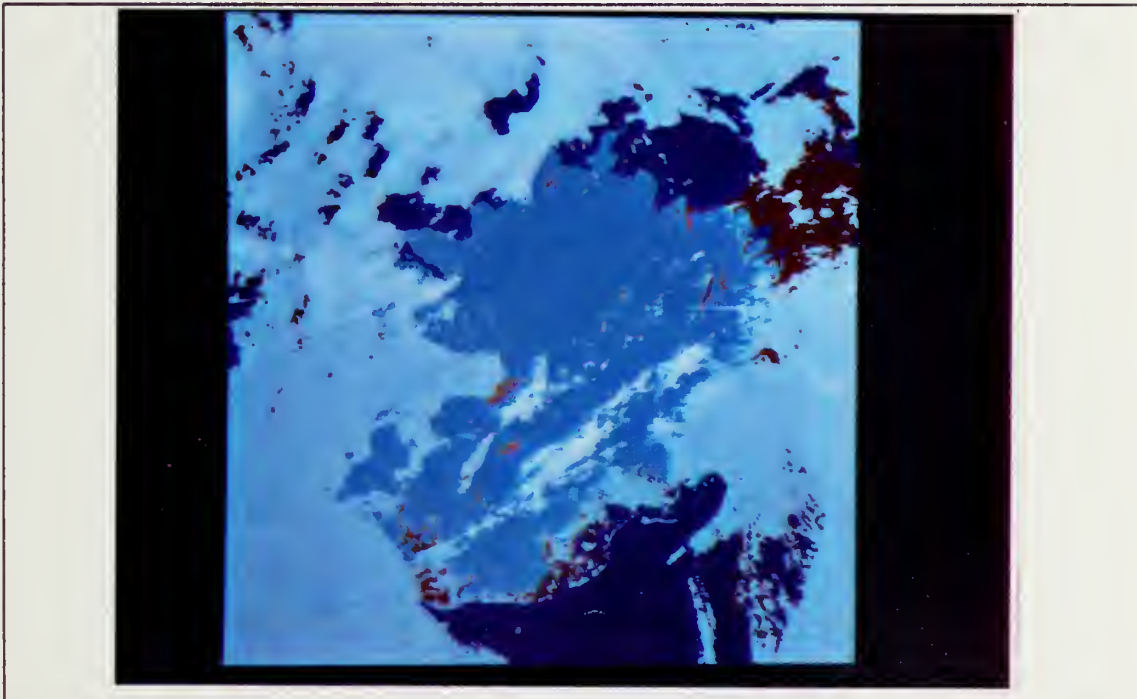
Fig. 4.2   Case 1 cloud analysis results.

Fig. 4.3   Case 2 cloud analysis results.

45

ambiguous. An examination of the channel 4 image reveals that this region is predominantly ocean, beneath a layer of thin cirrus. Another area of ambiguity occurs in the shadows of clouds cast upon the underlying snow. These scenes are similar to the preceding ambiguous ocean pixels in that they both exhibit nearly negligible reflectance in channel 2.

3. Case 3

The area of coverage in the Case 3 subscene is almost identical to that of Case 2. This NOAA-10 overview that encompasses Iceland and the adjacent ocean, was initiated at 1048 local time on 3 April 1987. In this subscene, a streak of thick cloud dominates the northeast portion of the island, while the remainder of the image is essentially cloud free. The analysis, shown in Fig. 4.4, depicts all but the most southern part of Iceland, as cloud covered. This is virtually impossible to detect from the channel 2 image alone. However, with the aid of the channel 4 image, a great deal of cirrus becomes evident. As before, the channel 3 reflectance reveals a greater extent of liquid cloud coverage than indicated in channel 2. Thus, while the significant amount of cloud cover depicted in the analysis is almost imperceptible in channel 2, it is substantiated by channels 3 and 4.

A graphic illustration of the technique's success is evident in the upper left corner of the subscene. In the channel 2 and channel 4 images, there is virtually no difference in either reflectance or brightness temperature between the surface in this corner and the obvious cloud coverage spanning northern Iceland. However, in the channel 3 image this surface nearly becomes invisible, in direct contrast to the highly reflective cloud cover over Iceland. Thus, the analysis identifies this section as snow or sea ice. An inspection of the overview verifies this area to be the southeastern extent of the fast ice attached to Greenland.

An entire section of red pixels stands out to the northwest of Iceland. An obvious linear discontinuity, in the form of a diagonal line, separates the ambiguous pixels from ocean pixels. Upon a detailed examination, this linear boundary was found to correlate with changes in the solar zenith angle. Apparently, the value of the solar zenith angle prior to the change, and its corresponding value of the anisotropic factor, were enough to prevent two matching scene classifications in succession. Thus, the current iterative method utilizing Taylor and Stowe's tabulated values of the anisotropic reflectance factor, is not without flaw. Currently, a smoothing technique is being tested that would interpolate the values of f, and thereby eliminate such sharp
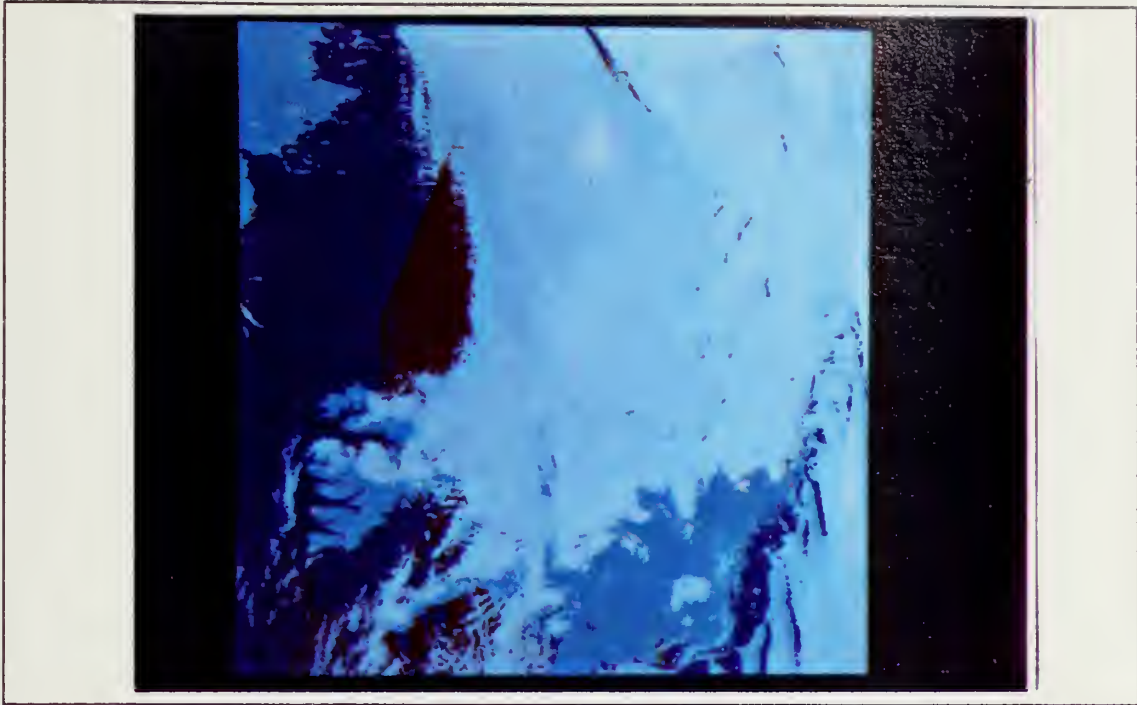
46

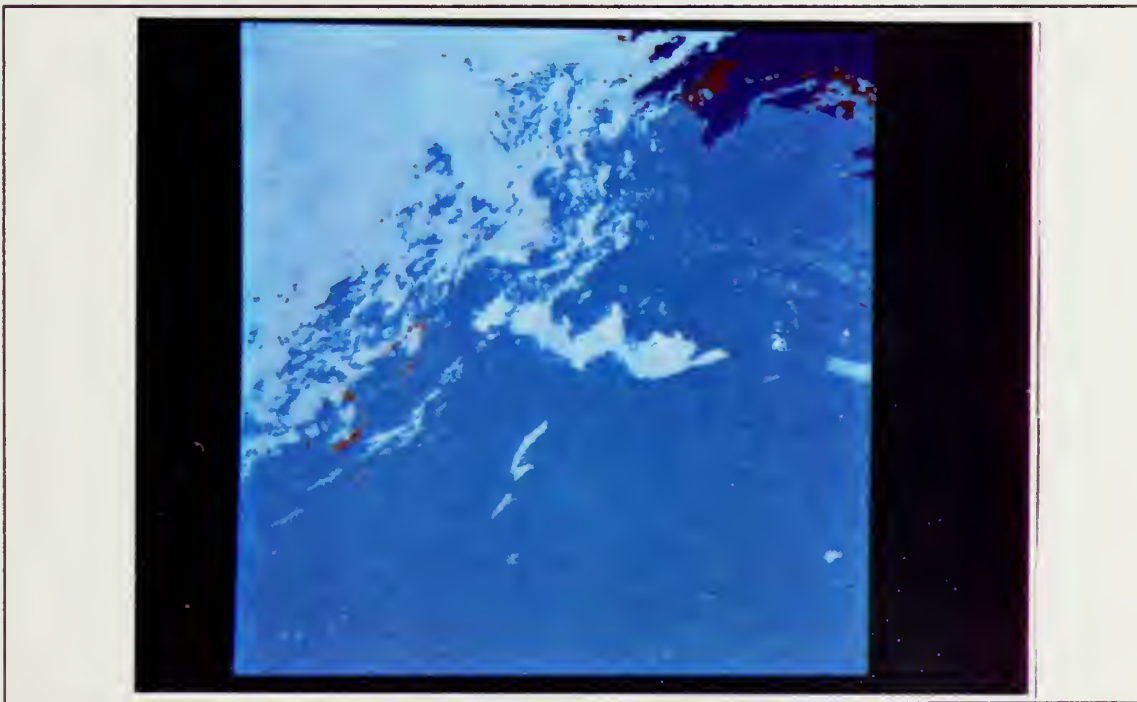Fig. 4.4   Case 3 cloud analysis results.

Fig. 4.5   Case 4 cloud analysis results.

discontinuities. Regardless, it is once again noteworthy to realize that the ambiguous pixels occur in areas that would otherwise be classified as ocean.

4. Case 4

Case 4 is extracted from the NOAA-10 pass that commenced at 0947 local time on 1 April 1987. This subscene is centered on the island of Spitzbergen. From the overview, it is clear that the upper left portion of the image is cloud covered. This concurs with the results of the analysis, which are pictured in Fig 4.5. The only other major area analyzed as cloud is found in the very center of the image. The cloud depicted here is not easily distinguished in either channel 2 or channel 4. However, it stands out in the channel 3 reflectance image. In the opposite sense, one feature that resembles cloud in the VIS and IR imagery, but does not display the requisite channel 3 reflectance, is a frozen bay located just to the right of the subscene center.

The amount of ambiguous pixels is quite small for this case. This is likely due to the fact that there is only a small area of ocean in the subscene. As expected, of the red pixels that do exist, most are located in this vicinity. For the most part, the rest of the analysis of this case is straightforward.

5. Case 5

The subscene for Case 5 is taken from the NOAA-10 overview that was initiated on 27 March 1987 at 1000 local time. The area of coverage extends from the east coast of Greenland, across a large expanse of fast ice, to the open ocean due north of Iceland. The analysis for this case is shown in Fig. 4.6. There are basically three significant types of cloud coverage depicted in this analysis. The lower right corner of the image accounts for a large section of low level, open cell clouds over the ocean. Near the center of the analysis, an isolated liquid cloud is obvious in the images of all three channels. The analysis has no difficulty identifying this feature. The third noteworthy type of cloud cover is harder to distinguish in the conventional VIS and IR images. It is located at the top of the subscene near the center, and also near the middle of the subscene, to the left. This cloud type resembles fog in channels 2 and 4, as it closely follows the topography of Greenland. However, only about half of this low level cloud registers a great enough channel 3 reflectance to be classified by the algorithm.

The number of ambiguous pixels in this subscene is practically negligible. However, a different problem, yet to be addressed, becomes apparent in this case study. Obvious pixels of snow covered land are being classified as ocean. This occurs in the
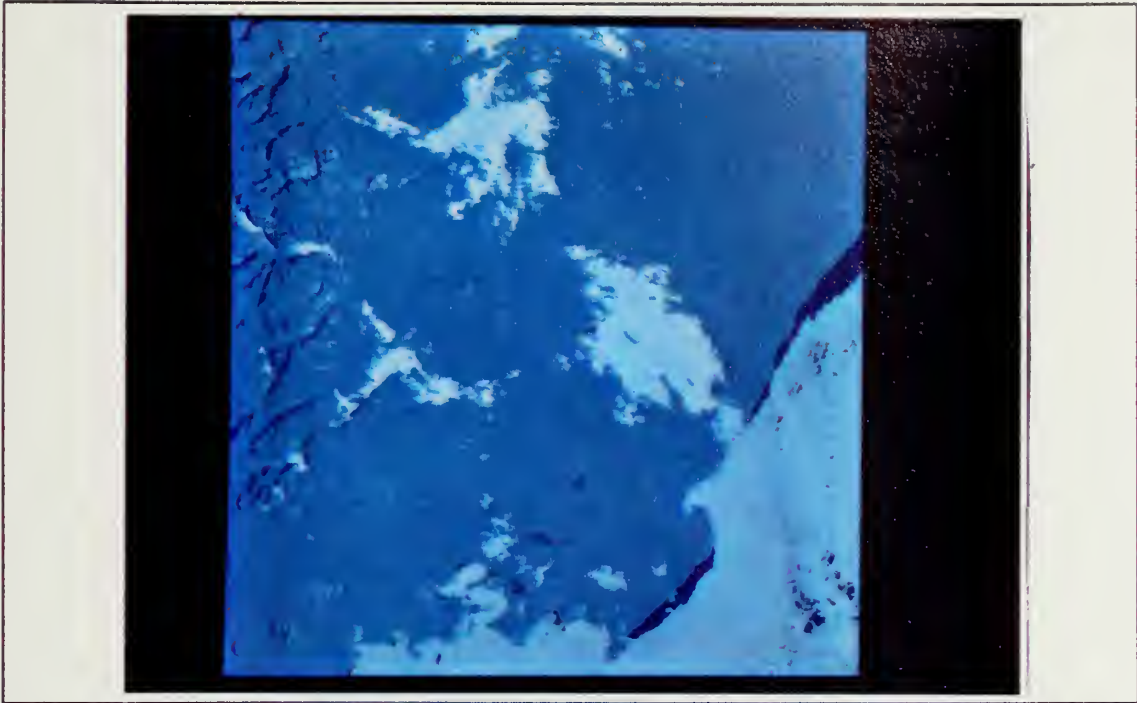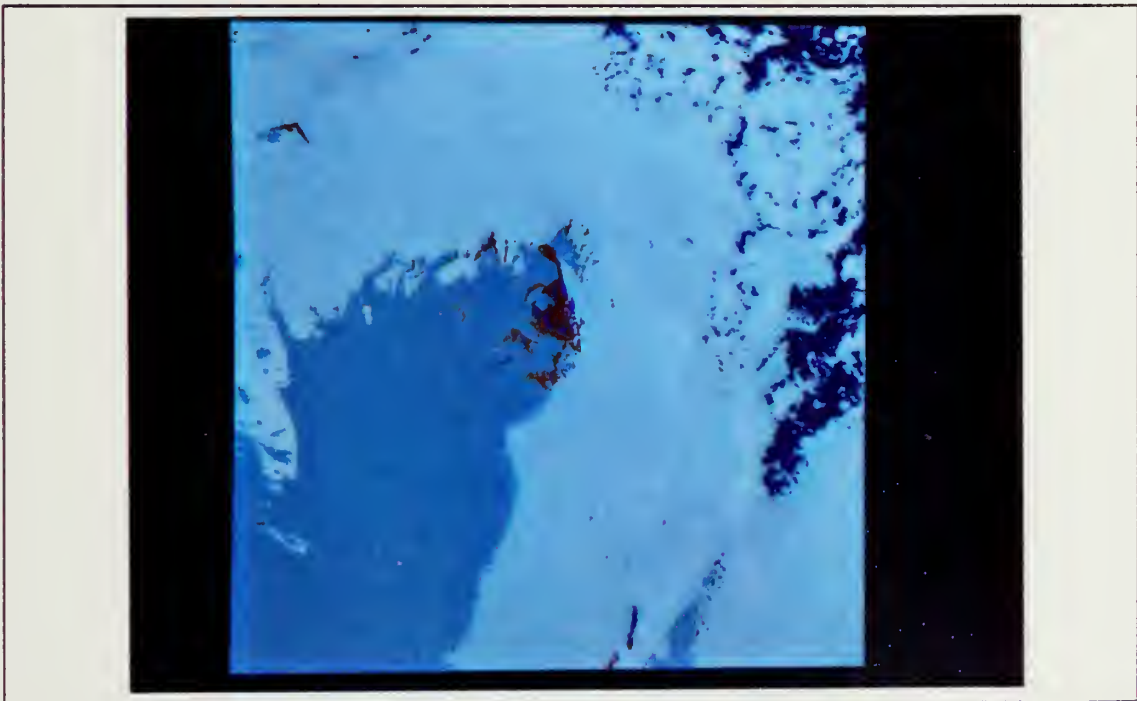
Fig. 4.6   Case 5 cloud analysis results.

Fig. 4.7   Case 6 cloud analysis results.

49

shadows of the topographic relief, and is a direct result of weak channel 2 reflectance in these areas. The low angle of the morning sun is not sufficient enough to illuminate the far side of the steep ridges, and so, the reflectance in channel 2 is not great enough to exceed the maximum threshold established for ocean pixel classification. This problem can be easily alleviated however. A simple reference to the location of any land with sharp relief can be subjectively applied to the routine. The topography of any sea ice that is not fixed to a specific geographical location, is not likely severe enough to cause this problem elsewhere.

6. Case 6

The Case 6 subscene is centered over the outer edge of the fast ice located east of Greenland. This case was taken from the NOAA-10 pass that started at 1042 local time on 25 March 1987. From the overview, a region of low level cloud cover is visible over the ocean. It extends across the ice edge at the top and right side of the image. The analysis, pictured in Fig. 4.7, detects this cloud deck over the ocean, as well as over the ice. The extent of cloud coverage in this scene is substantiated by all three images. From the channel 2 image, the cloud cover can be perceived by differences in texture. In the channel 4 image, higher temperatures separate this cloud from the colder underlying ice. However, the greatest contrast is evident in the channel 3 reflectance image, which is logically used to define the extent of cloud coverage in the analysis.

The only ambiguous pixels are located in the center of the analysis image. This is an ocean area dominated by ice fragments, under cloud free conditions. Interestingly, the vast area of ocean in the upper right corner of the image does not contain any ambiguous scenes. Overall, the scene classification in this case is not too complicated.

D. EVALUATION OF THE ANALYSIS

1. Statistical Comparison

The previous qualitative, case by case description of the analysis does not provide a true measure of the overall effectiveness of the routine. This section attempts to accomplish this through a statistical comparison of the subjective 'ground truth' results to the corresponding cloud analysis results. A general synopsis of the scene classifications that the routine handled well, and a description of the scene types that presented problems, are also included in this section.

50

The same 216 points that were initially classified by the experts, were also classified by the analysis. The acetate grid that had been utilized by the analysts (refer to Fig. &grid), was applied to each 6.5 x 6.5 inch, color coded image of the analysis results. The cloud analysis scene classifications that resulted were subsequently subjected to the same boundary criteria (within a 1.0 mm radius) as the subjective results. This yielded both exact results, and results with boundaries. Therefore, the analysis statistics are divided into the categories of exact matching cases, and cases with boundaries included.

Of the 131 scenes that the subjective analysts identified without a discrepancy or boundary, the analysis classified 102 of these identically. This equates to a 77.9% success rate. The analysis scenes that did not concur with the 'ground truth' included cases of exact disagreement, and cases classified as boundaries by the algorithm. Only four instances of exact disagreement occurred, compared to 25 instances of boundary classification. Of course, the four cases of exact disagreement are considered misclassifications. The 25 analysis scenes classified as a boundary were further checked to ensure that at least one of the elements matched the corresponding classification of the experts. All 25 scenes met these criteria. Therefore, for statistical purposes, these scenes are included with the expanded boundary case data base.

The number of scenes in the expanded boundary category data base is 183. Besides comprising all of the exact match cases, these data include three separate boundary groups. The first, as described above, are cases in which the analysis classified the scene as a boundary, but the experts did not. There are 25 of these. The second group is comprised of cases in which at least one of the analysts classified the scene as a boundary, but the algorithm did not. There are 23 of these. Finally, the third group of boundary cases includes scenes which were classified as a boundary by both the analysis and at least one expert. There are 29 of these. It should be reemphasized that all of the scenes in the above boundary groups met the 1.0 mm radius criterion. The total number of exact matches, exact boundary matches and cases in which at least one element of the boundary concurred with the ultimate classification is 179. This relates to a 97.8% success rate. Such a percentage reflects the rather liberal restrictions imposed on the acceptance of boundary case classifications. Therefore, credence in this figure should not be as strong as that for the more realistic 77.9% success rate of the smaller, exact case data base.

The number of ambiguous scenes that correspond to the 216 total grid points, is 22. This amounts to 10.2%. A breakdown of the subjective categorizations pertaining to these scenes is as follows:

- 11 ocean, or boundary between ocean and liquid cloud.
- 3 ice cloud.
- 3 rejected due to disagreement among the analysts.
- 5 other.

Of the four scenes definitely misclassified, three are identified as ice cloud by the analysts, but categorized as snow/sea ice by the algorithm. The other scene is an ocean pixel incorrectly analyzed as ambiguous. Table 4 summarizes the comparison of results between the cloud analysis algorithm and the 'ground truth' provided by the experts.

TABLE 4

STATISTICAL RESULTS OF THE ANALYSIS

Cases of exact agreement	102/131	77.9%
Cases of misclassification	4/131	3.1%
Agreement with boundaries	179/183	97.8%
Total ambiguous cases	22/216	10.2%

2. General Evaluation

Some generalizations can be made concerning the overall effectiveness of the cloud analysis routine. The routine has no difficulty in identifying liquid cloud cover over the snow and sea ice. The contrast in the channel 3 reflectance is substantial enough to delineate even the thinnest low clouds in this situation. However, the analysis routine has trouble with the classification of optically thin, liquid cloud over the ocean. In this type of scenario, the tendency is to overestimate the cloud cover. Some ocean scenes that appear to be cloud free in channels 2 and 4, nonetheless, exhibit a high channel 3 reflectance, and are consequently identified as cloud. If the channel 2 and channel 4 scenes appear to be cloud free because the image quality is

poor, and are in fact affected by the presence of thin cloud, then this is not a problem. However, if the scenes are truly cloud free, then the channel 3 threshold for identifying clouds is too low, and should be raised.

As with Allen's analysis, this routine displays limited success in identifying ice clouds over snow and sea ice. In many cases, the extent of ice cloud, which is clearly evident from the infrared image of channel 4, is underestimated. The cirrus streaks in Cases 1 and 2, are proof of this problem. Also, while the number of incorrect classifications is minimal, it is no coincidence that most of these misclassifications are identified as ice cloud by the experts, but classified as the snow or sea ice background by the analysis routine. The effectiveness of the temperature factor is hard to estimate in post analysis. The cirrus streaks identified in the Case 1 and Case 2 analyses qualitatively appear to be more extensive than they do in the channel 3 reflectance images alone. This evidence supports an increase in the identification of ice cloud pixels due to the differences in brightness temperatures and the use of the temperature factor. However, once again, a lack of image quality may be responsible for the apparent differences of ice cloud coverage between the analyses and the channel 3 images.

The iterative technique designed to identify ambiguous scenes needs improvement. The problems addressed in Case 3 are enough to justify a modification. The breakdown of the ambiguous cases does afford some insight into the problems encountered. As previously indicated, most of the ambiguous cases are either ocean or thin cloud over ocean scenes. Additionally, a cursory screening of the red pixels that do not actually fall under the grid points reveals that they rarely occur in locations other than at the boundaries or edges of ocean pixels.

A discussion of the algorithm thresholds sheds some additional light on the nature of the scenes classified as ambiguous. The initial channel 2 reflectance thresholds utilized for ocean pixel separation, were much closer to the theoretical estimates (approximately 0.10). However, these resulted in far too many cases of ambiguity. During the algorithm development process, it was found that increasing this value of the maximum channel 2 reflectance for ocean scene classification yielded a decreased number of ambiguous cases. As explained in Chapter III, the threshold of 0.45 was eventually found to produce the best overall classification results. The number of ocean pixels classified was increased, but not significantly, since these pixels also had to satisfy the conditions of a channel 3 reflectance less than 0.05. At the same time, the number of ambiguous pixels decreased. Now, while channel 2 reflectance values greater

than 0.45 further reduce the number of ambiguous scenes, they do result in other problems. Shadows on the ice and snow are too often classified as ocean pixels. Even at the current threshold of 0.45, this still poses a slight problem (refer to the discussion of Case 5, in the previous section). All things considered, the channel 2 reflectance threshold of 0.45 was established to afford the greatest accuracy in overall scene classification.

The relationship between the anisotropic reflectance factor iteration and the channel 2 reflectance threshold for ocean scenes, is obviously the driving force behind the number of ambiguous pixels identified. Because of the aforementioned interrelationships and complexities inherent to the separation scheme, it is difficult to identify any one factor that can be attributed to ultimately determining an ambiguous pixel. However, a detailed examination of the red pixels reveals that many occur in ocean areas with minimal channel 3 reflectance (likely less than 0.05) and fairly significant channel 2 reflectance (likely greater than 0.45). This type of scene is not initially classified as ocean, but rather defaulted to a cloud classification. The subsequent iterations, starting with an anisotropic reflectance factor for cloud, continually change the classification and ultimately lead to the ambiguous scene designation.

In Chapter III, it was theorized that the ambiguous cases may aid in the identification of optically thin clouds. As it turns out, even the thinnest wisps of liquid cloud meet the channel 3 reflectance threshold, and are identified anyway. However, the ambiguous pixels may possibly be useful in identifying the thin ice clouds over ocean. These clouds reflect nicely in channel 2, but minimally in channel 3. The red pixels in the upper right corner of Case 2 correlate to scenes that fit this scenario. Thus, the value of the ambiguous pixels may not be limited to simply identifying cases of anisotropic reflectance uncertainty, but may also aid in the identification of some of the ice cloud. In any case, the method of determining ambiguous pixels is not certain, and can stand some improvement, if for no other reason than to eliminate the solar zenith angle induced discontinuities addressed in Case 3.

All in all, the analysis routine does a commendable job in distinguishing cloud cover from the arctic backgrounds. The verification of the analysis results, by an arguably small data base of 'ground truth', yields noteworthy success rate statistics. Minor flaws in ice cloud discrimination and ambiguous pixel classification do exist, but these conditions are not enough to overcome the success of an automated technique that positively and objectively identifies liquid cloud over snow and ice.

54

V. SUMMARY AND RECOMMENDATIONS

An objective cloud analysis routine, initially developed by Allen (1987), has been modified, and applied to satellite data from the Arctic, in an attempt to solve the difficult problem of discriminating cloud cover from the snow and sea ice backgrounds. The routine is based on a multispectral approach which utilizes channels 2, 3 and 4 of the AVHRR sensor onboard the polar-orbiting NOAA satellite series. Previous objective means of separating cloud cover from snow and ice, using the conventional VIS and IR imagery, have failed due to a lack of sufficient contrast at these wavelengths. However, this technique exploits the stark reflectance contrasts available in channel 3 (NIR) to identify arctic clouds with a high degree of success. The process isolates the channel 3 reflectance contribution from the total channel 3 radiance measurement, by subtracting the thermal emission component which has been approximated from the temperature of the channel 4 radiance measurement. The derived channel 3 reflectance is significant for liquid clouds and ice clouds with small crystals, while it is negligible for snow and sea ice. This allows a threshold to be set, which easily discriminates the two surface types. The only difficulty in separation occurs for ice clouds with large crystals (on the order of the particle radii for snow and sea ice). Fortunately, many of these clouds can be identified by differences in transmissive characteristics between channels 3 and 4. However, this secondary method of separation is only effective for a limited range of optical depths, which prevents some ice clouds from being identified at all.

The automated cloud analysis routine was tested on six separate case studies. Results of the analyses were then compared to 'ground truth', which had been established subjectively by three independent experts. An initial comparison of results yielded an impressive 77.9% success rate when applied to a small, but uncontroversial data base (131 points). Results were also compared to a larger data set of 183 points, which included some points of contention among the analysts. The success rate for this was 97.8%. However, this is a dubious figure when considering the liberal standards for data point selection.

While the promise of the technique is without question, there were some problems encountered. These include:

1. The incomplete identification of ice clouds, which has just been addressed.

2. The possible overestimation of liquid cloud over ocean. In many cases, the extent of cloud defined by the channel 3 reflectance and the cloud analysis, exceeded that of the conventional VIS and IR images. While this may be attributed to inadequate photographic quality in the areas of thin cloud and weaker contrasts for channels 2 and 4, it is still not safe to rule out a deficiency in the channel 3 reflectance derivation process.

3. A significant portion of scenes, comprised of thin cloud over ocean, were identified as ambiguous. These were ambiguous in that a particular anisotropic reflectance factor could not be prescribed that would positively identify the scene as either ocean or cloud.

4. The iterative method of determining the ambiguous pixels was, in itself, deficient. The dependence of the tabulated factors for anisotropic reflectance on solar zenith angle, was such that some scene classifications were suddenly and distinctly identified as ambiguous, simply by changes in solar zenith angle.

5. The misclassification of some snow pixels located in shadows of topography also tainted the results of the analysis. In an effort to lessen the extent of ambiguous cases, the channel 2 reflectance threshold for ocean scene classification was set artificially high, thereby creating this problem.

6. The noise which is inherent to channel 3 of the AVHRR and amplified in the arctic environment, appeared in the analysis' results as scenes of cloud in incongruous vertical bands. While this only occurred in the vicinity of actual, coincident cloud scenes, and because it is easily recognizable, this is not a significant drawback. Anyway, this is beyond the control of the algorithm. It should be noted that this noise has diminished with the launching of each new NOAA satellite. Noticeable differences are even apparent between the NOAA-9 and NOAA-10 images analyzed in this study.

In lieu of the aforementioned problems and the questionable credibility of the statistics, the following recommendations are presented:

1. Further study should be undertaken to determine the effectiveness of utilizing the unique sets of anisotropic reflectance factors, especially at high solar zenith angles. While the technique utilized in this thesis represents an improvement of simply using an average anisotropic reflectance factor for all possible surfaces, the relatively large number of ambiguous cases indicates that there may be better ways of assigning the correct factor to each pixel to be classified. Also, Taylor and Stowe's (1984) tabulated values are self admittedly not as comprehensive at the high relative azimuths and solar zenith angles associated with the polar regions. This lack of data likely contributes to the linear discontinuities of the ambiguous cases which arise from changes in the solar zenith angle. In the meantime, the smoothing technique mentioned in the description of Case 3, should be perfected. Interpolation of the values will add more credibility to the scene classifications.

2. More work should be concentrated on the areas of possible liquid cloud overestimation. These predominantly ocean scenes which exhibit a high channel

3 reflectance and a low channel 2 reflectance, may or may not contain liquid cloud. While the channel 3 reflectance technique may be so sensitive that it can successfully identify even the thinnest sea smoke or arctic haze, it is unlikely. In any case, surface based observations would be of great assistance in confirming the true sky conditions. If, in fact, the algorithm is overestimating the extent of cloud cover, an added stipulation of a minimum channel 2 reflectance threshold could be easily employed to limit the number of cloud classifications over water.

3. The possibility of using specific temperature thresholds for ice cloud identification should be investigated. The differences in transmissivity in channels 3 and 4 could be only exploited for a limited range of optical thicknesses, and consequently the temperature factor threshold met with limited success in identifying ice clouds. A technique that can detect differences in surface temperatures may be more capable of separating the ice cloud from the arctic backgrounds. Raschke *et al.* (1987) define channel 4 temperature ranges for the various arctic surfaces. Values for snow are from 240 - 265 K, while sea ice is more discrete at 268 - 270 K, and ice clouds are less than 255 K. Although an obvious overlap exists between snow and ice cloud, a threshold can be set to separate sea ice and the warmer snow from ice cloud. It may prove to be more successful than the current temperature factor.

4. The present analysis routine should be applied to a larger data base and subjected to verification by 'ground truth' derived from objective means. Of the 216 total points, only 131 were useable without question. To add more credence to the statistics, a much larger data set is necessary. Similarly, the data for this study were taken from one experiment, conducted in the same geographical vicinity, within a time period spanning less than three weeks. Future studies should use samples from different locations and different times of the year. The procedure of verification should include coincident surface observations of sky cover. While the view from the surface may be different from that of the satellite, this form of 'ground truth' is indispensable in confirming the subjective determination of cloud cover. The method of subjective analysis could also be improved. Firstly, the acetate placement should be standardized among the analysts. Secondly, more stringent requirements on the classification of boundaries should be employed (reduce the radius or FOV). Lastly, the criteria used to select eligible boundary scenes should be more restrictive.

Overall, the analysis tested in this thesis performs quite capably in resolving the previously difficult matter of arctic cloud discrimination. In a routine such as this, the true worth of derived reflectance in the NIR is unquestionably demonstrated. Although future satellites are designed to incorporate a 1.6 μm channel for snow/cloud discrimination, the knowledge and experience gained from applications at 3.7 μm will certainly prove useful in developing and testing new software since the reflective properties at these wavelengths are very similar.

57

APPENDIX
SATELLITE IMAGES

This appendix serves as a convenient location to consolidate all the satellite images from each of the six cases that are discussed in the text of the thesis. Included in this section are the following:

-   Overview channel 2 reflectance (0.87 μm).
-   Subscene channel 2 reflectance (0.87 μm).
-   Subscene channel 4 thermal emission (11.0 μm).
-   Subscene channel 3 reflectance (3.7 μm).
-   Subscene cloud separation algorithm.
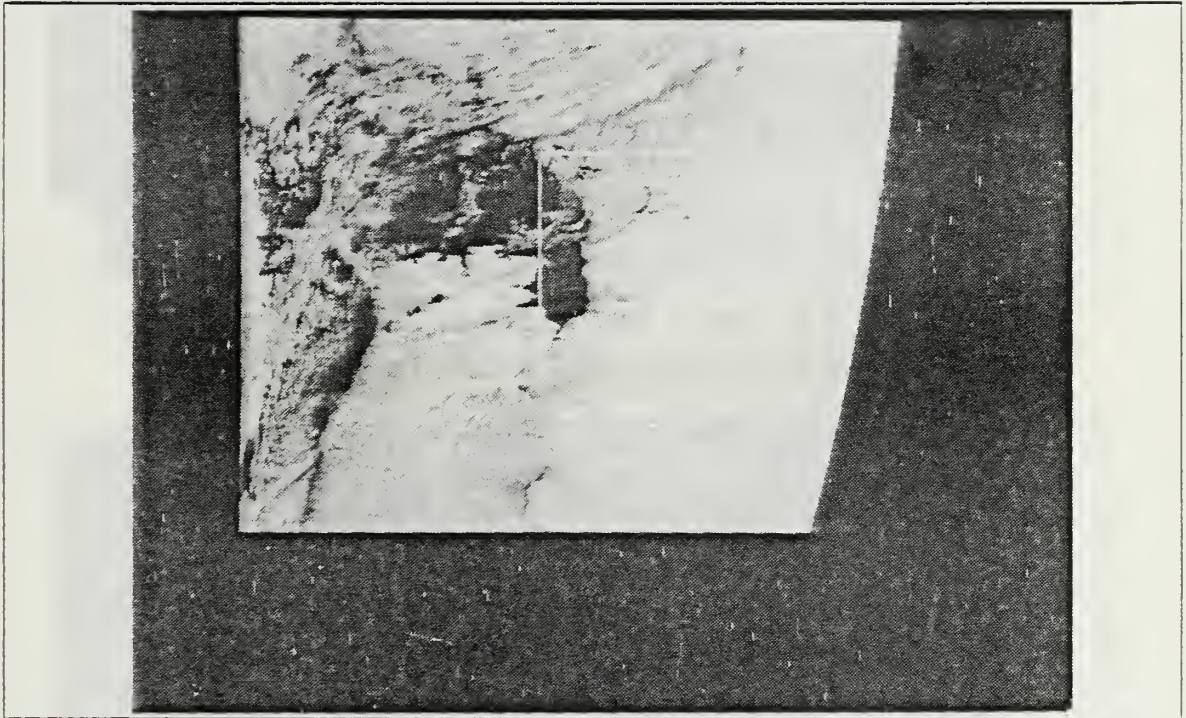
Fig. A.1 Case 1: 1042, 25 Mar 1987, channel 2 overview.
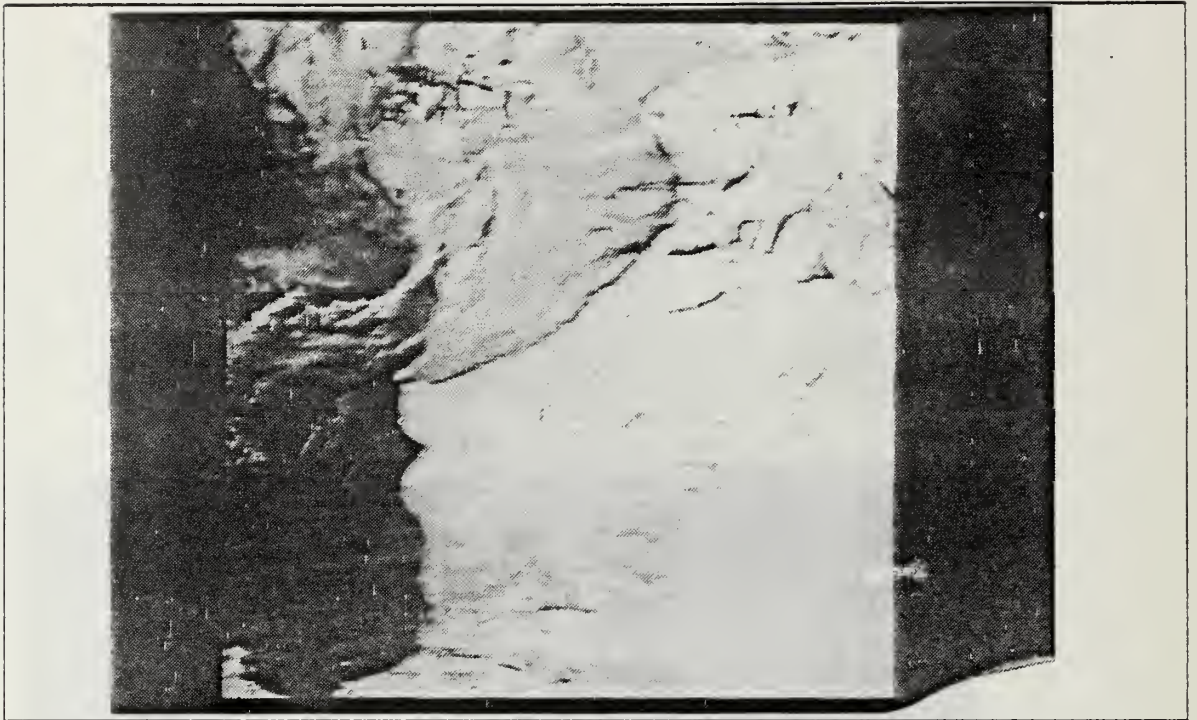
Fig. A.2 Case 1: 1042, 25 Mar 1987, channel 2 subscene.

Fig. A.3 Case 1: 1042, 25 Mar 1987, channel 4 subscene.
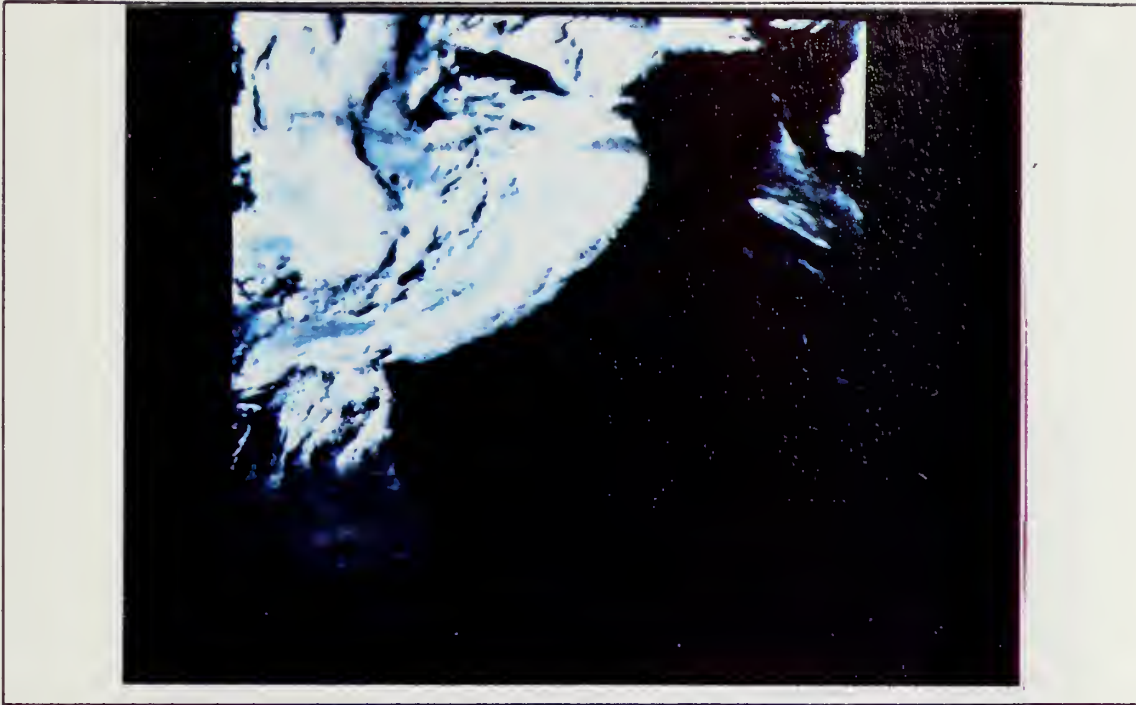
Fig. A.4   Case 1: 25 Mar 1042, Channel 3 subscene.
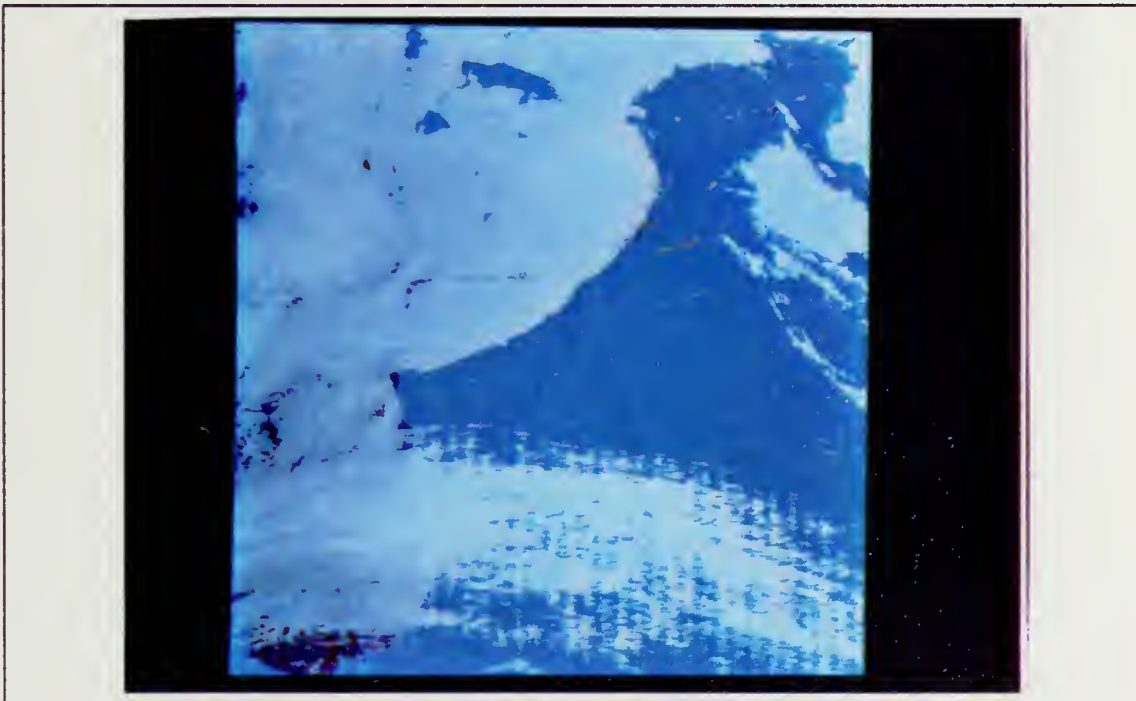
Fig. A.5   Case 1: 25 Mar 1042, Analysis results.
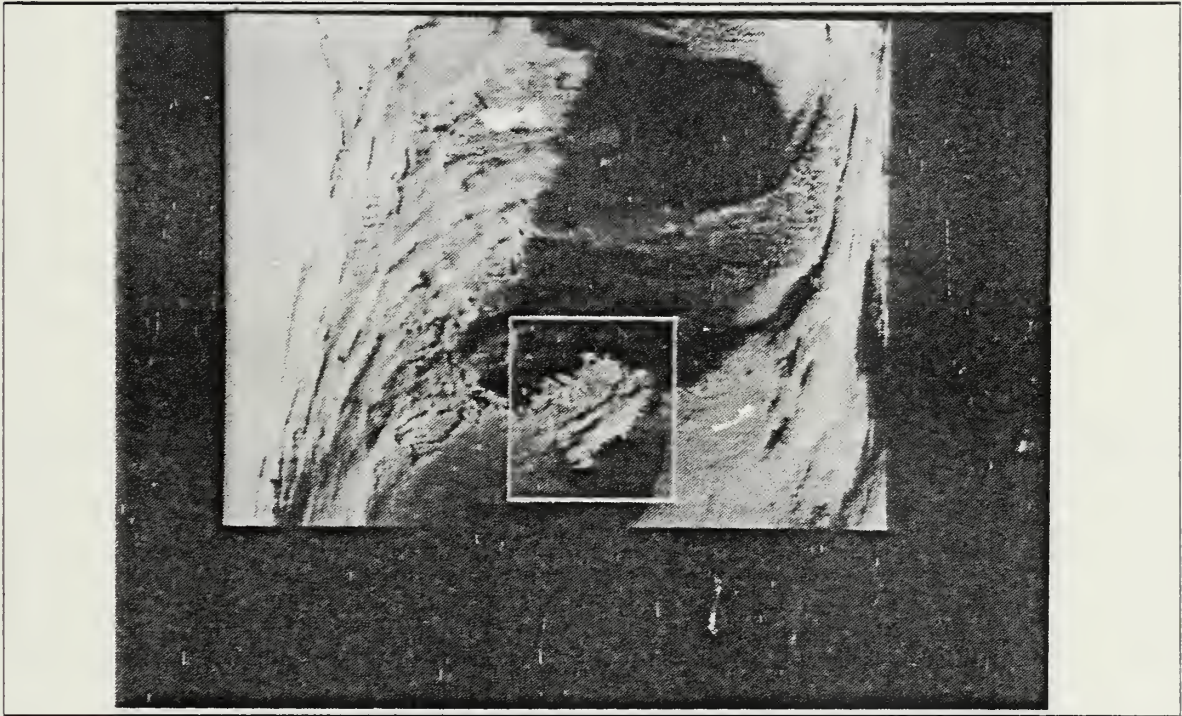
Fig. A.6   Case 2: 1000, 27 Mar 1987, channel 2 overview.
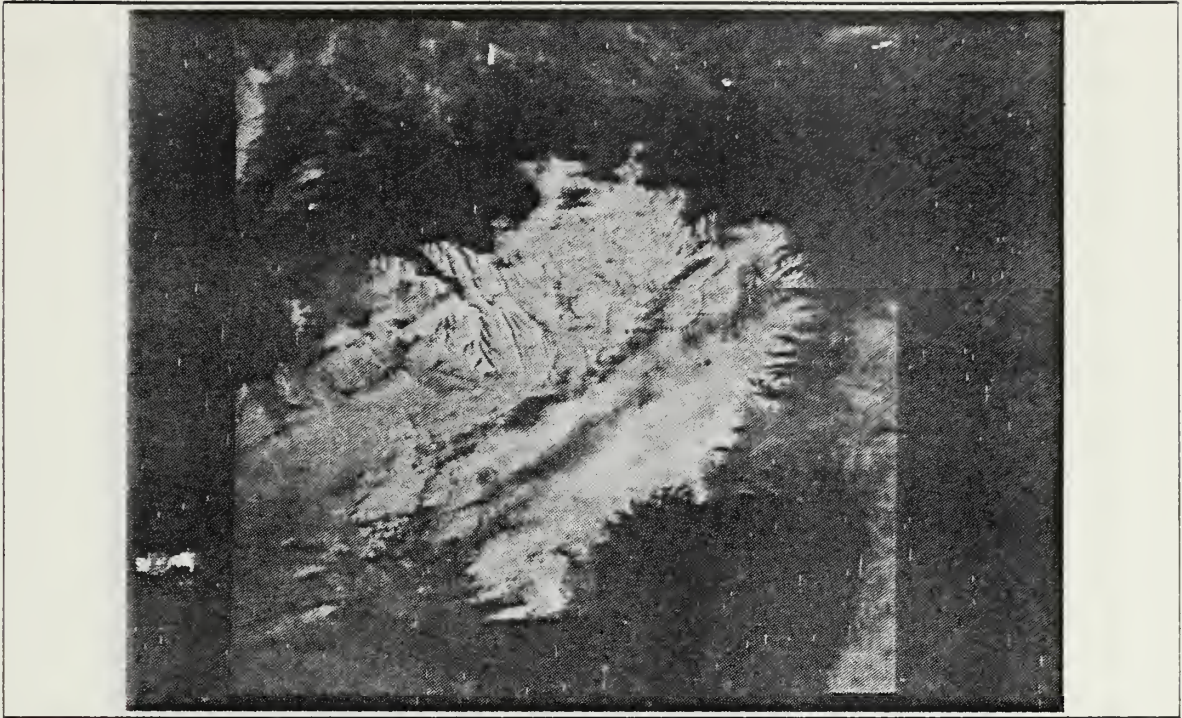
Fig. A.7   Case 2: 1000, 27 Mar 1987, channel 2 subscene.
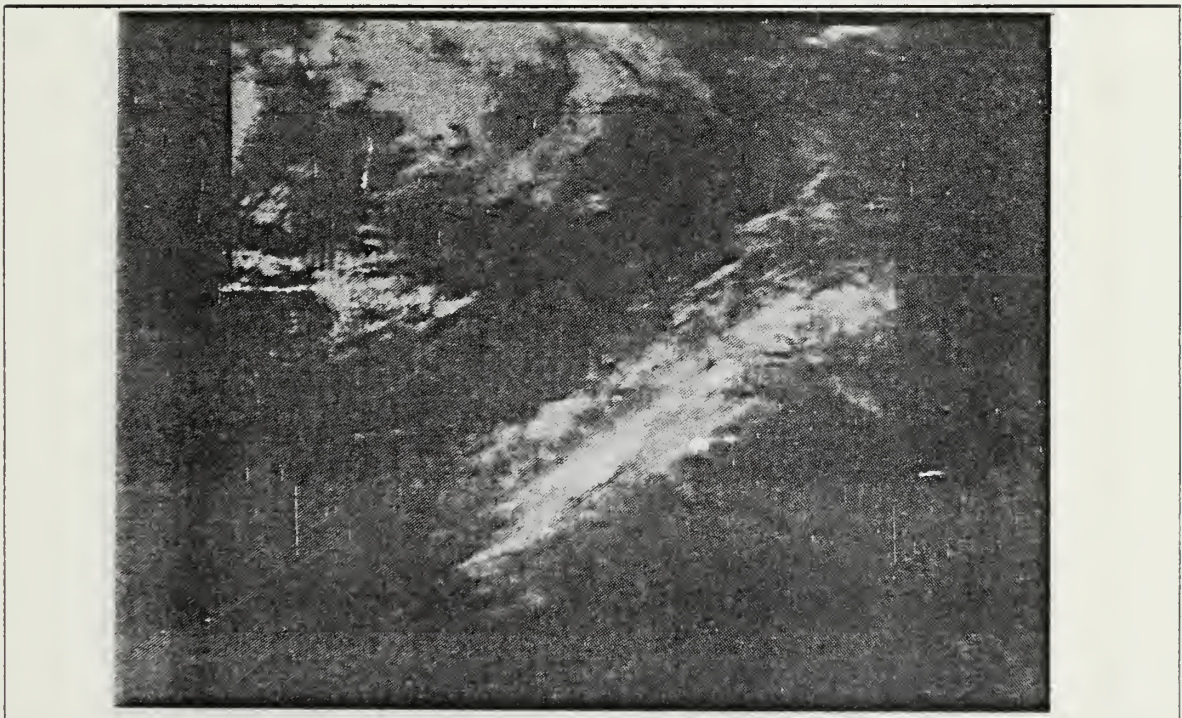
Fig. A.8   Case 2: 1000, 27 Mar 1987, channel 4 subscene.
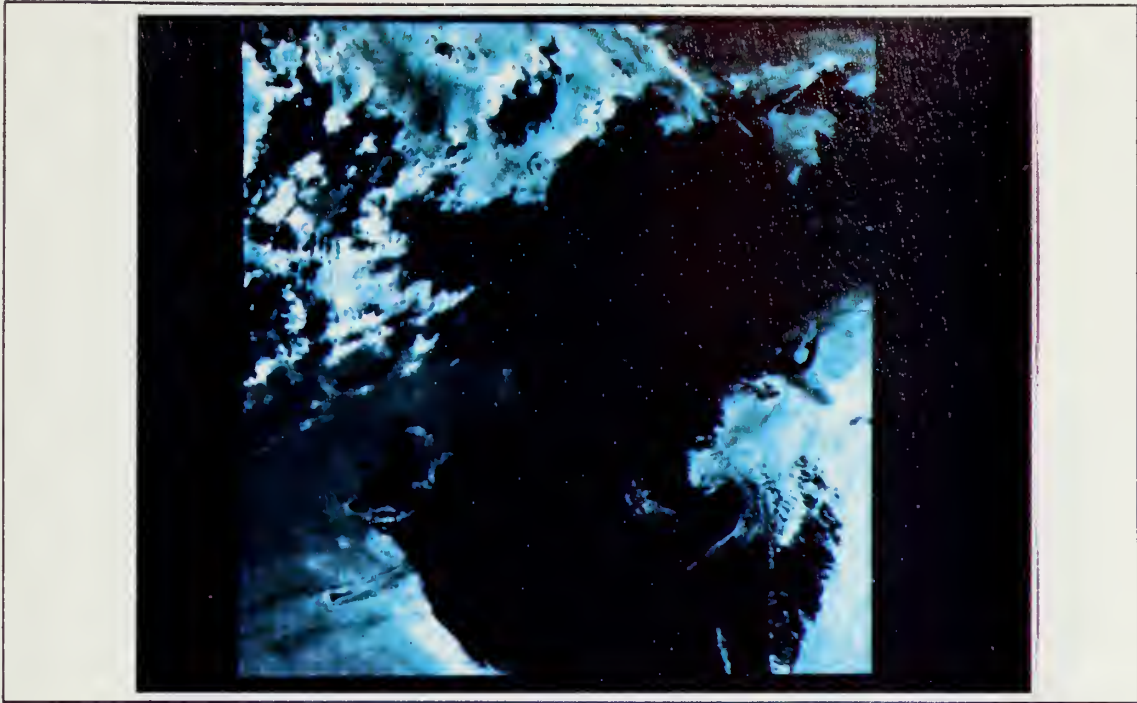
Fig. A.9   Case 2: 27 Mar 1000, Channel 3 subscene.
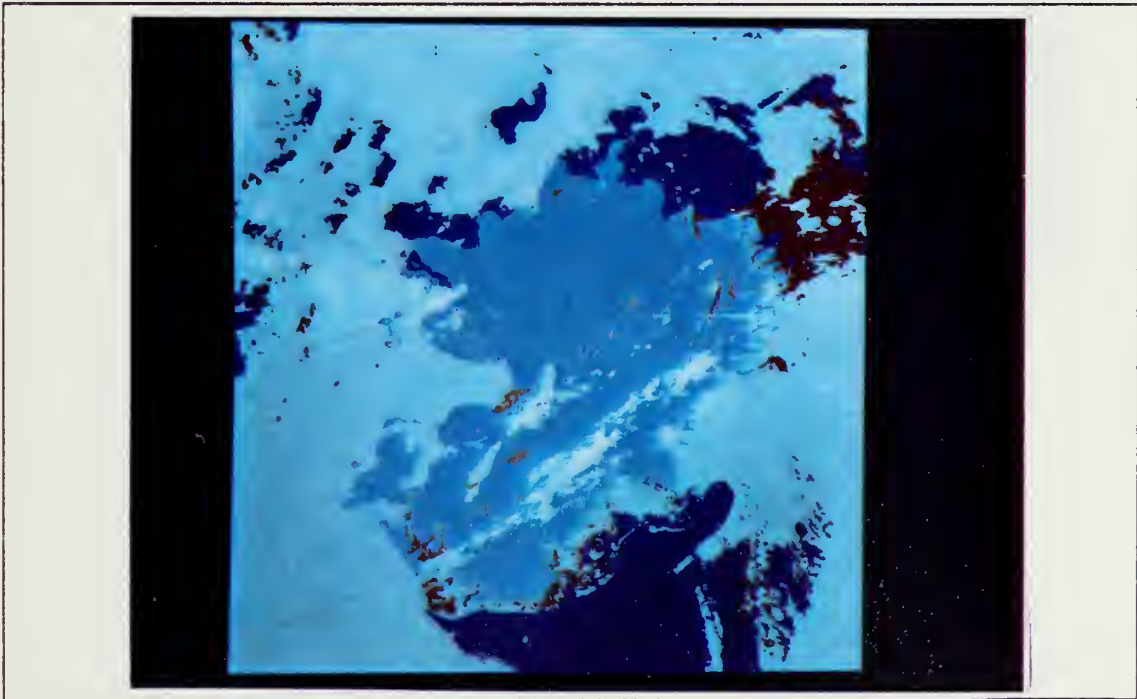

Fig. A.10   Case 2: 27 Mar 1000, Analysis results.
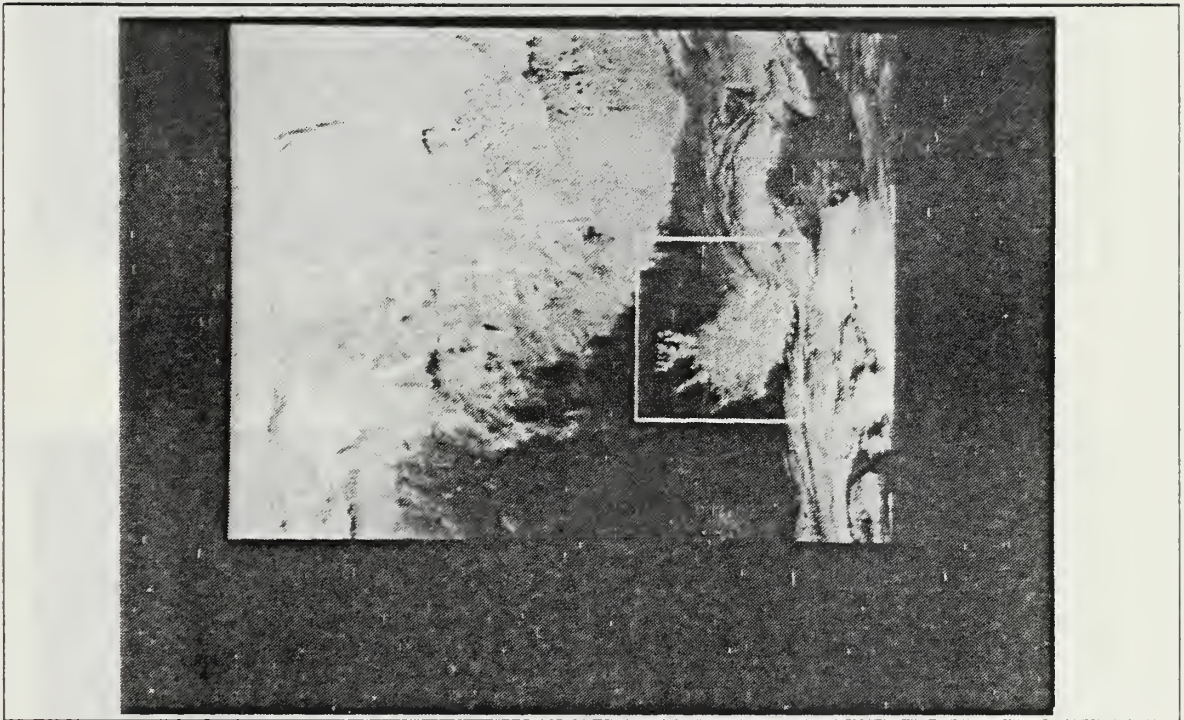
Fig. A.11   Case 3: 0947, 01 Apr 1987, channel 2 overview.
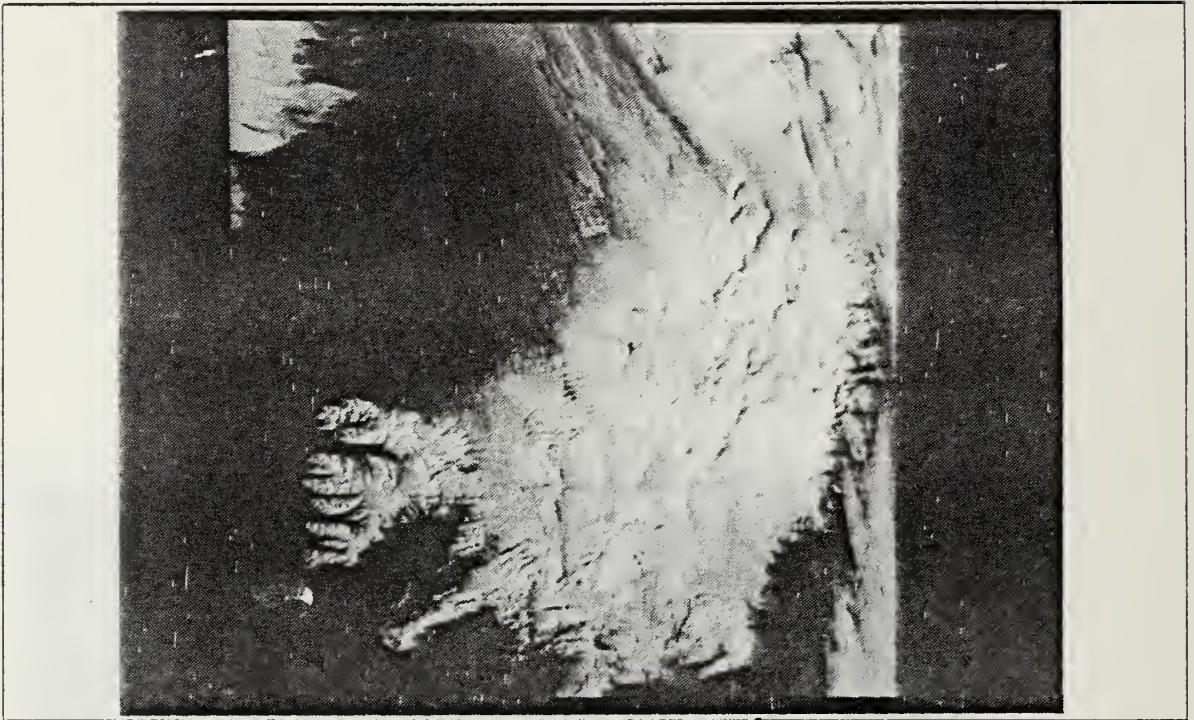
Fig. A.12   Case 3: 0947, 01 Apr 1987, channel 2 subscene.

Fig. A.13   Case 3: 0947, 01 Apr 1987, channel 4 subscene.
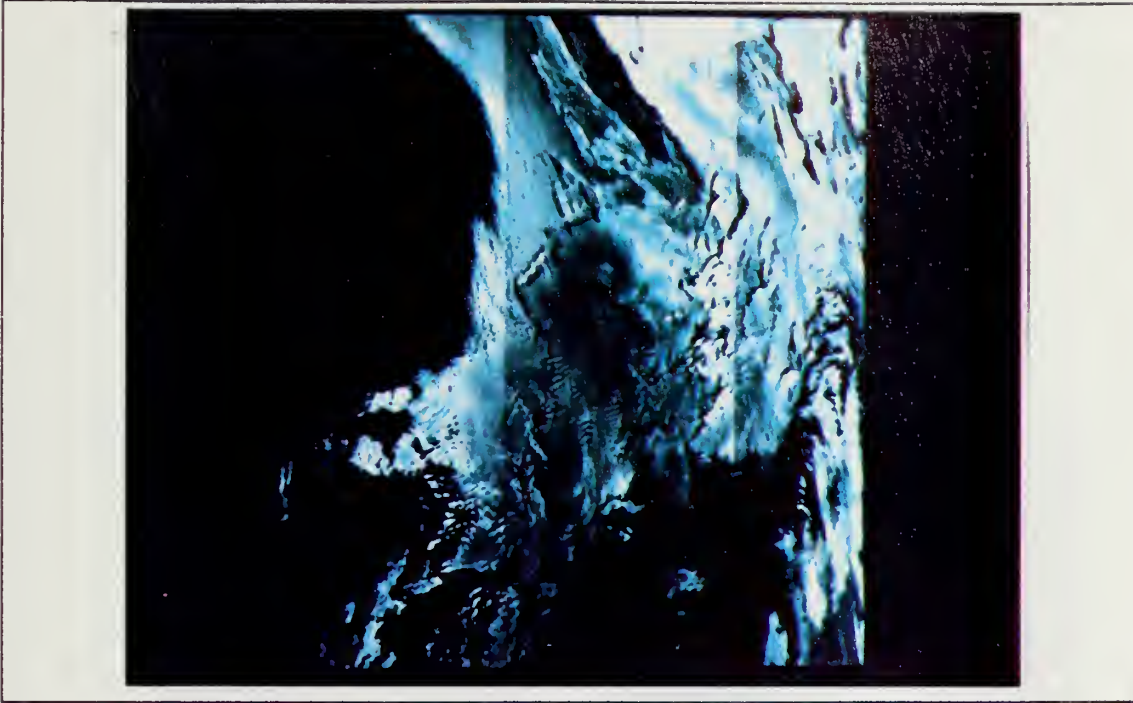
Fig. A.14   Case 3: 01 Apr 0947, Channel 3 subscene.
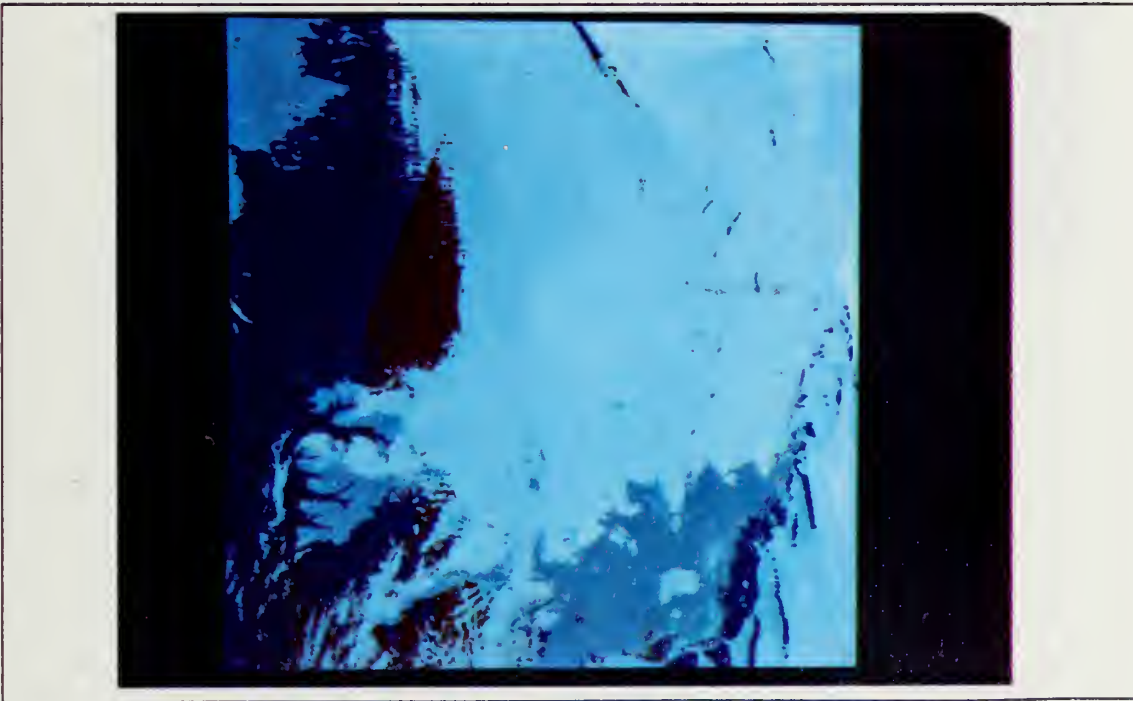
Fig. A.15   Case 3: 01 Apr 0947, Analysis results.
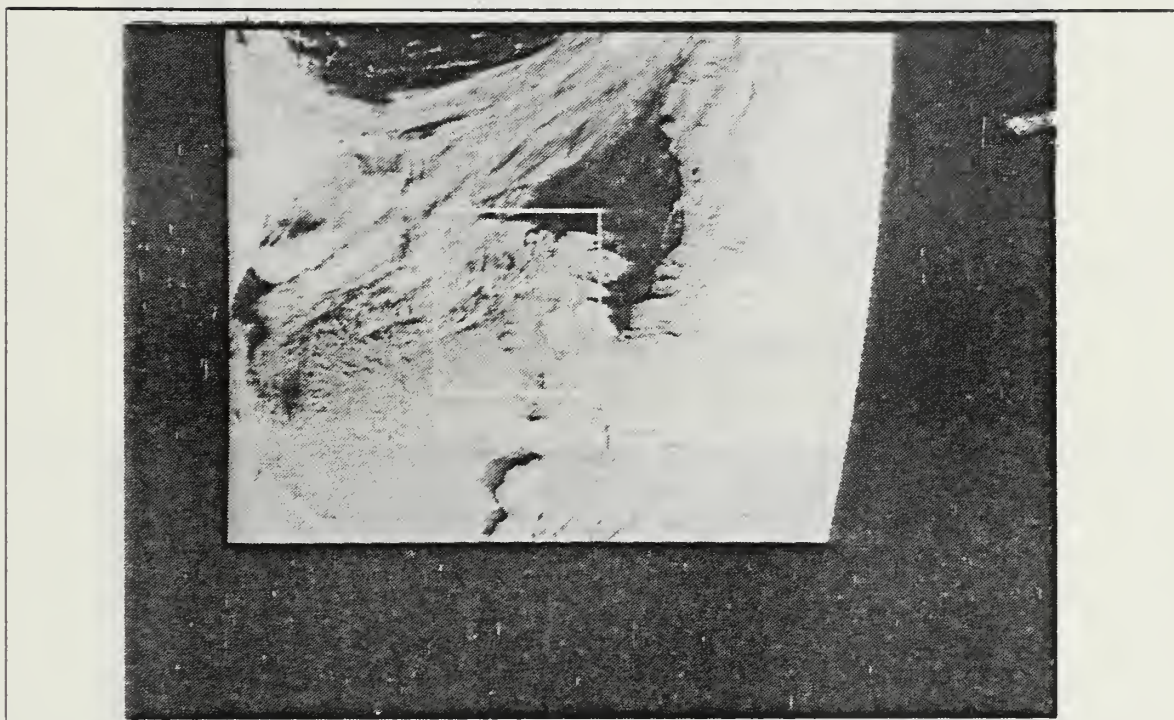
Fig. A.16   Case 4: 1048, 03 Apr 1987, channel 2 overview.
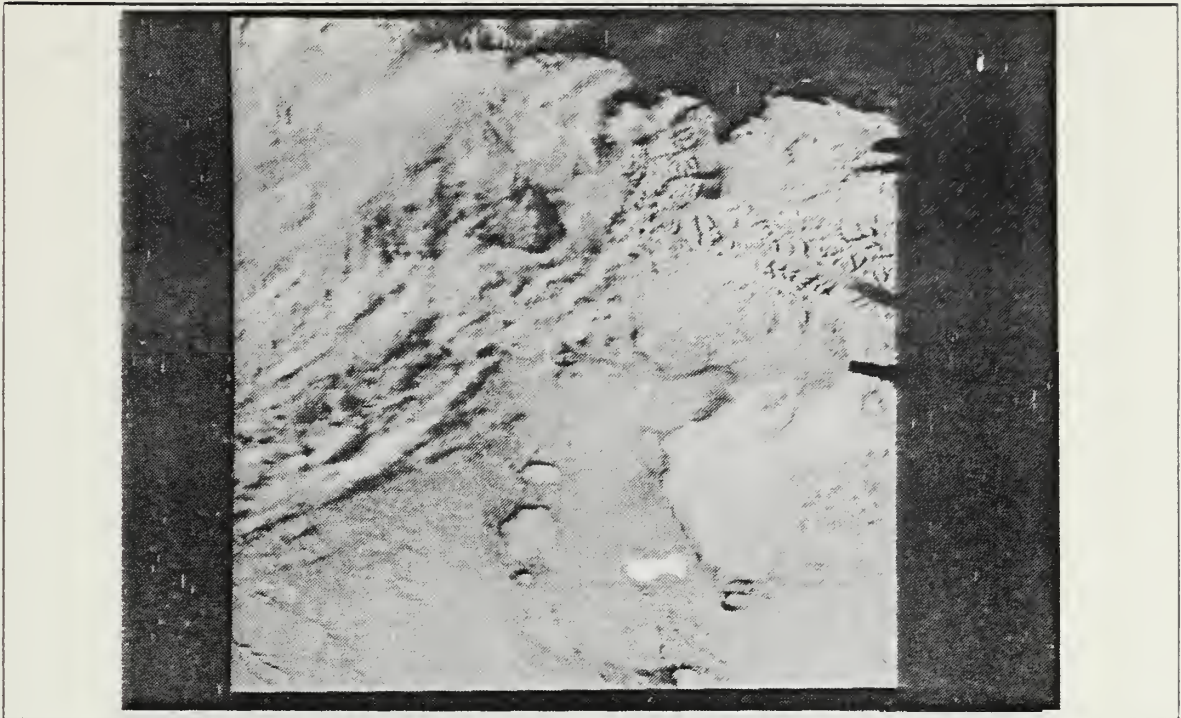
Fig. A.17   Case 4: 1048, 03 Apr 1987, channel 2 subscene.
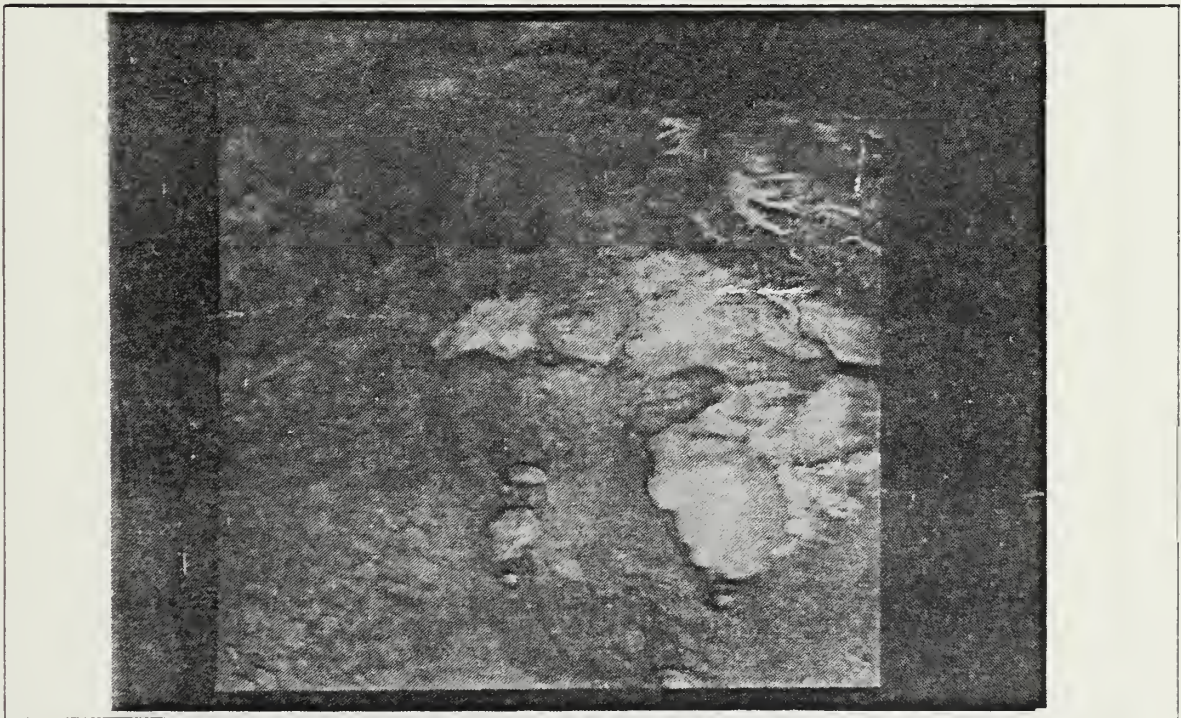
Fig. A.18   Case 4: 1048, 03 Apr 1987, channel 4 subscene.
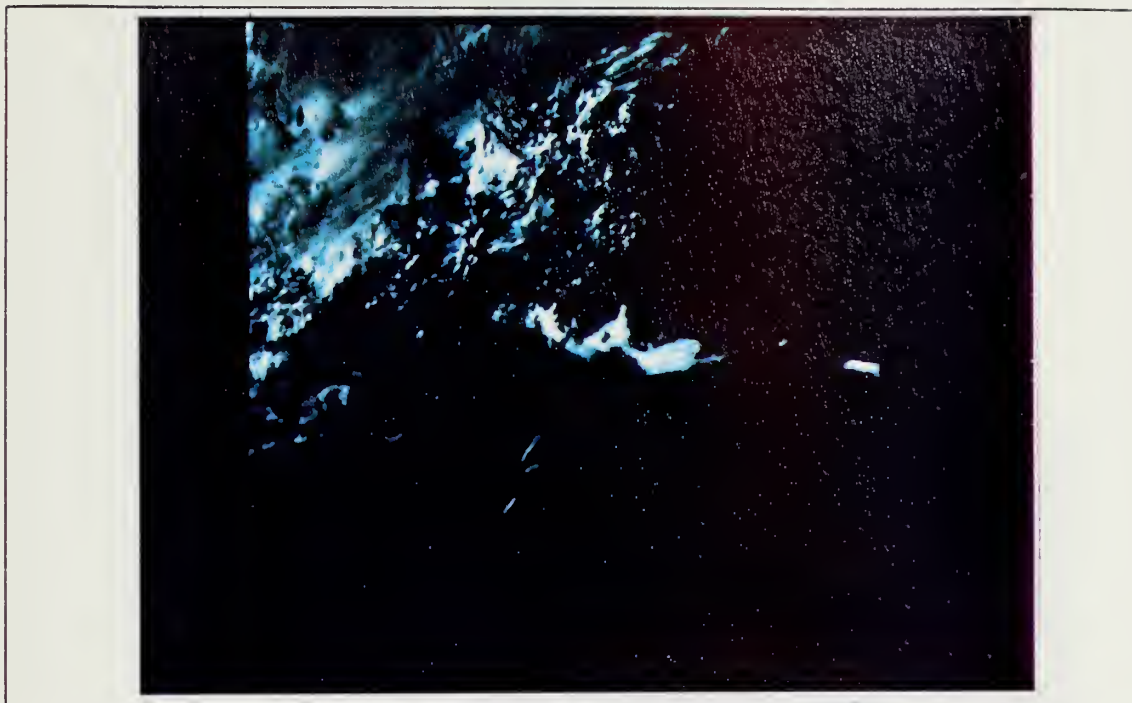
Fig. A.19   Case 4: 03 Apr 1048, Channel 3 subscene.
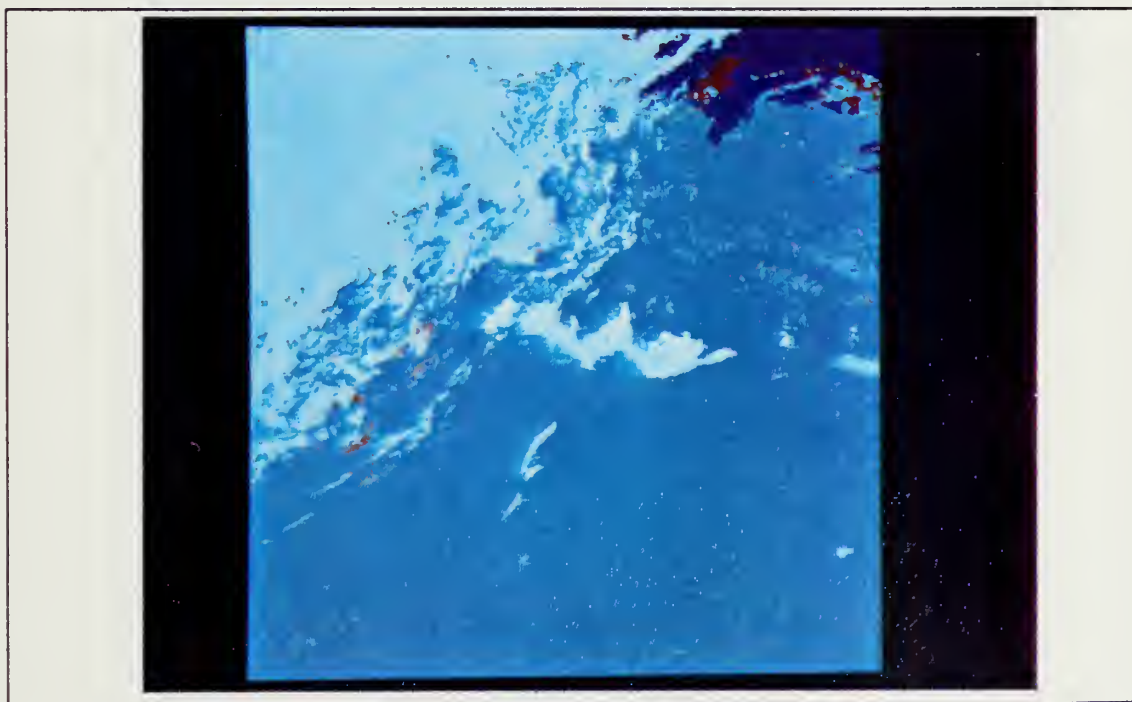
Fig. A.20   Case 4: 03 Apr 1048, Analysis results.
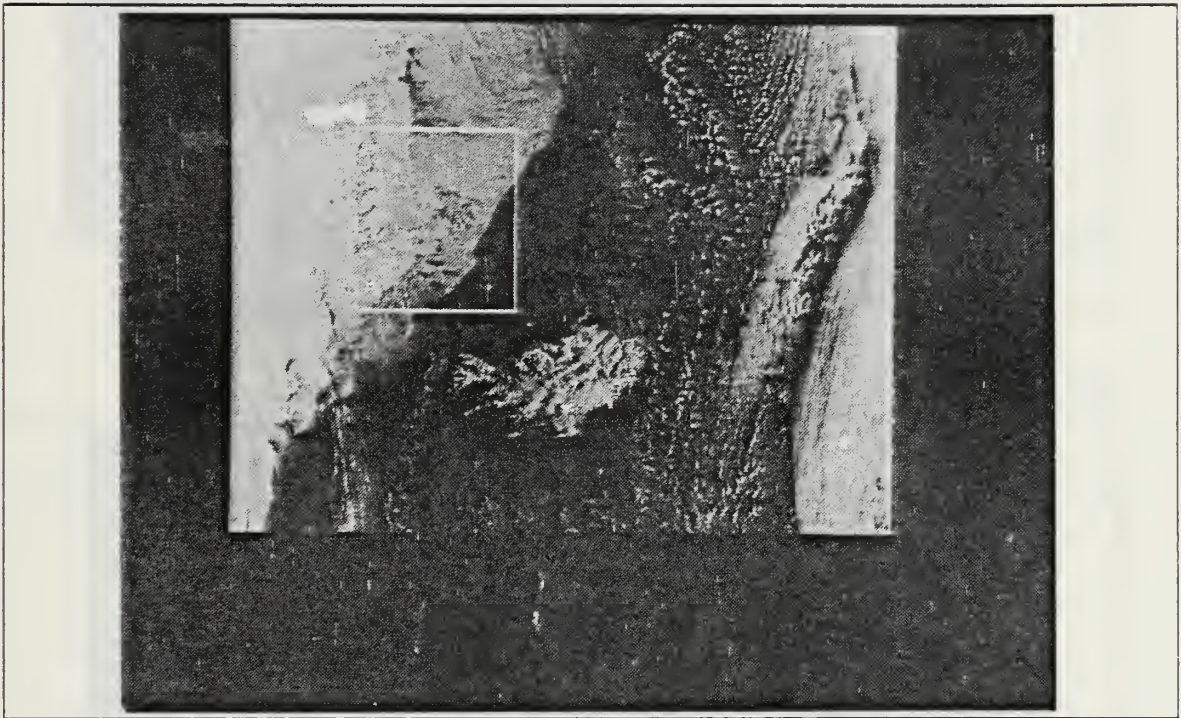
Fig. A.21 Case 5: 1004, 05 Apr 1987, channel 2 overview.
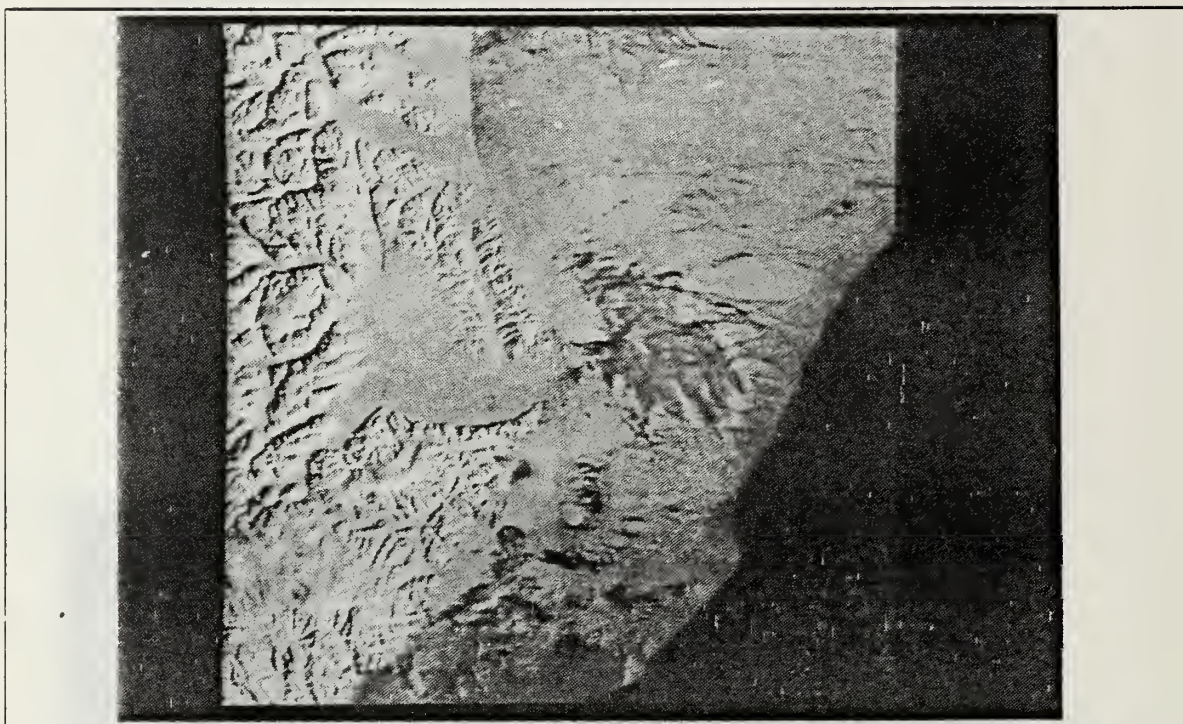
Fig. A.22   Case 5: 1004, 05 Apr 1987, channel 2 subscene.
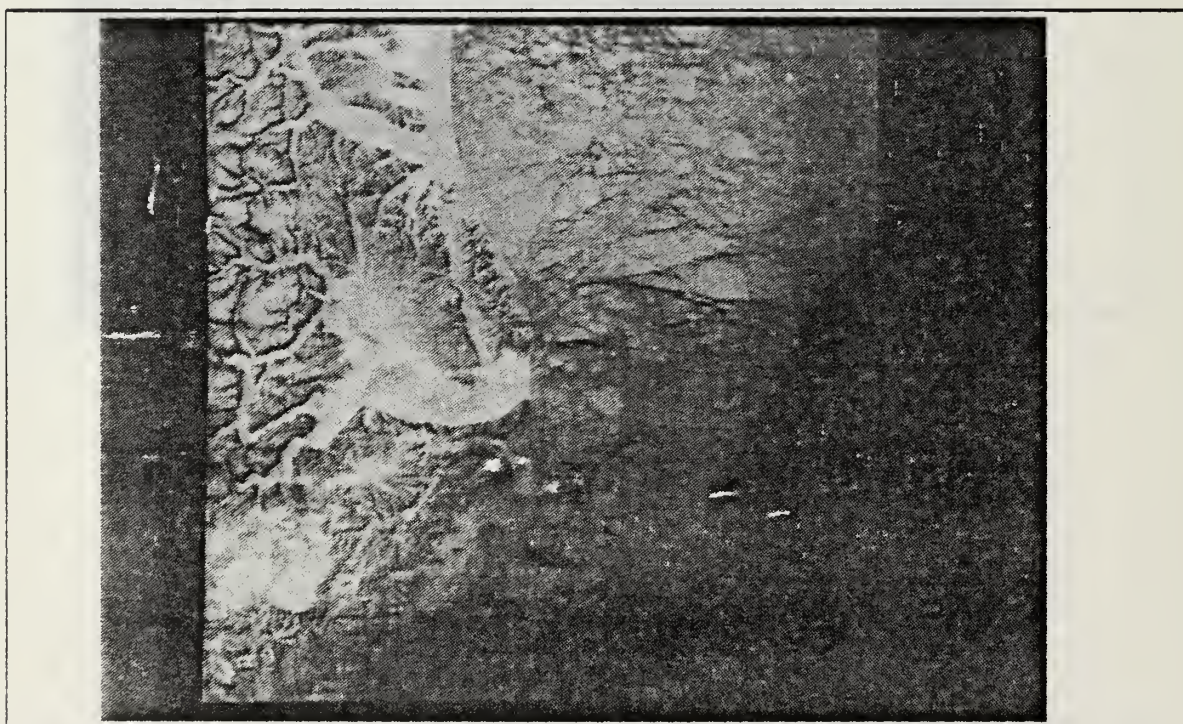
Fig. A.23   Case 5: 1004, 05 Apr 1987, channel 4 subscene.

Fig. A.24 Case 5: 05 Apr 1004, Channel 3 subscene.
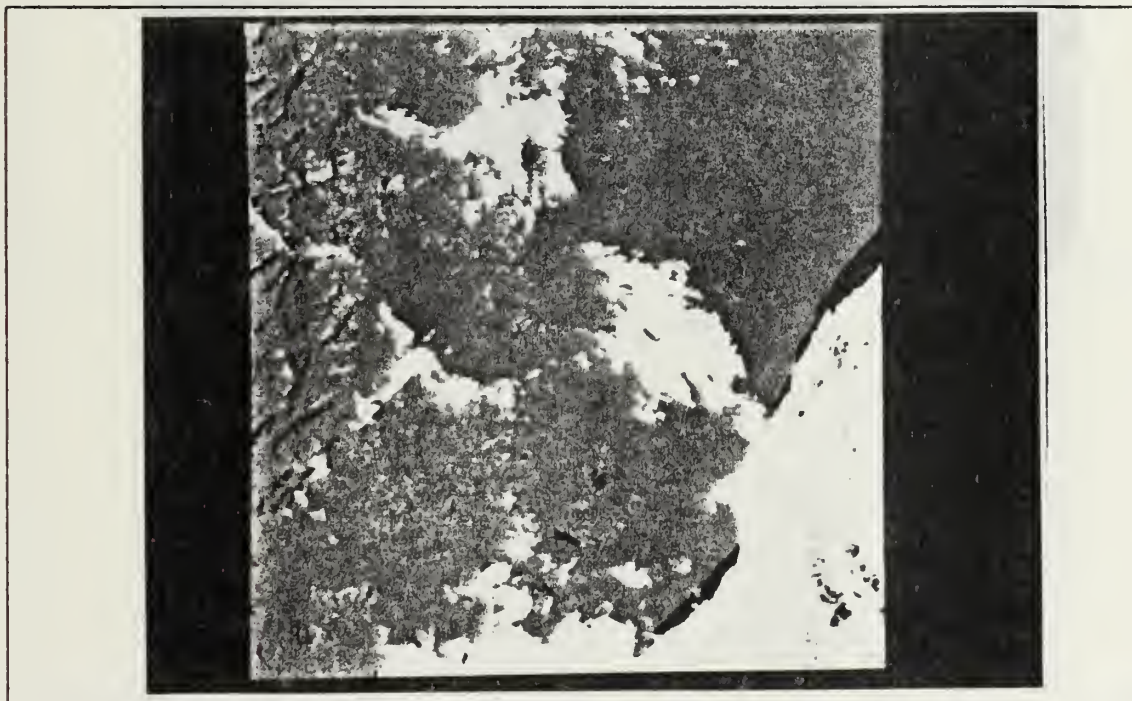
Fig. A.25 Case 5: 05 Apr 1004, Analysis results.

73
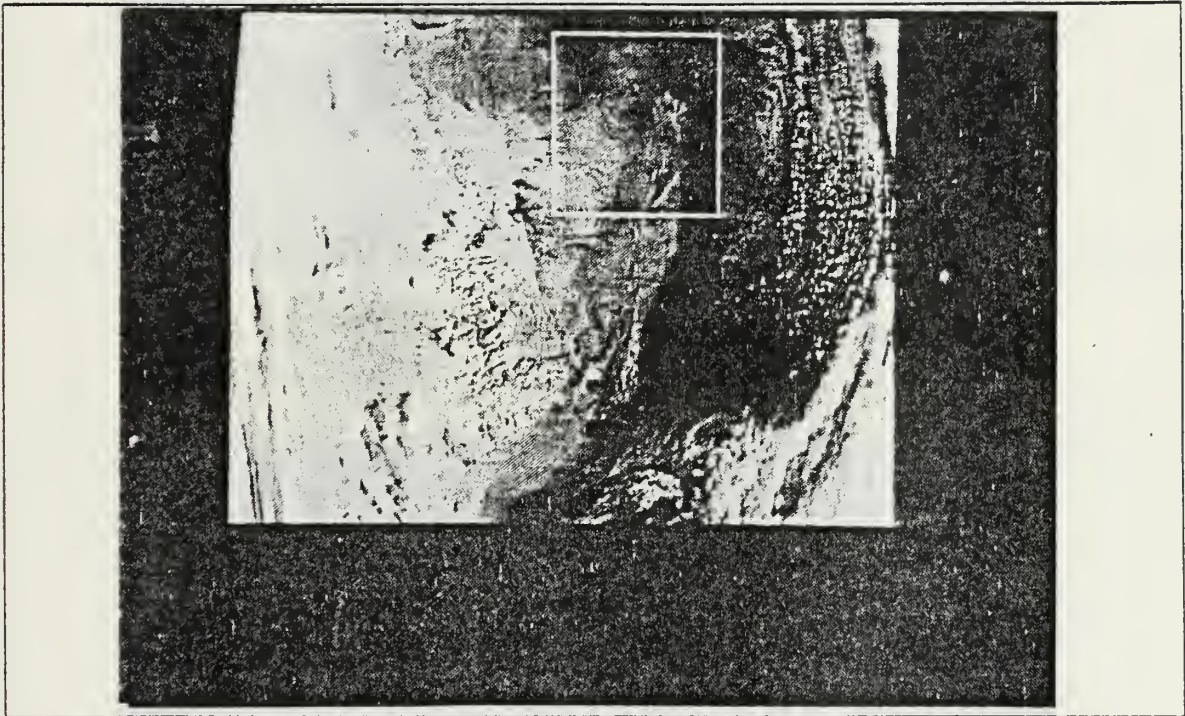
Fig. A.26   Case 6: 1119, 06 Apr 1987, channel 2 overview.
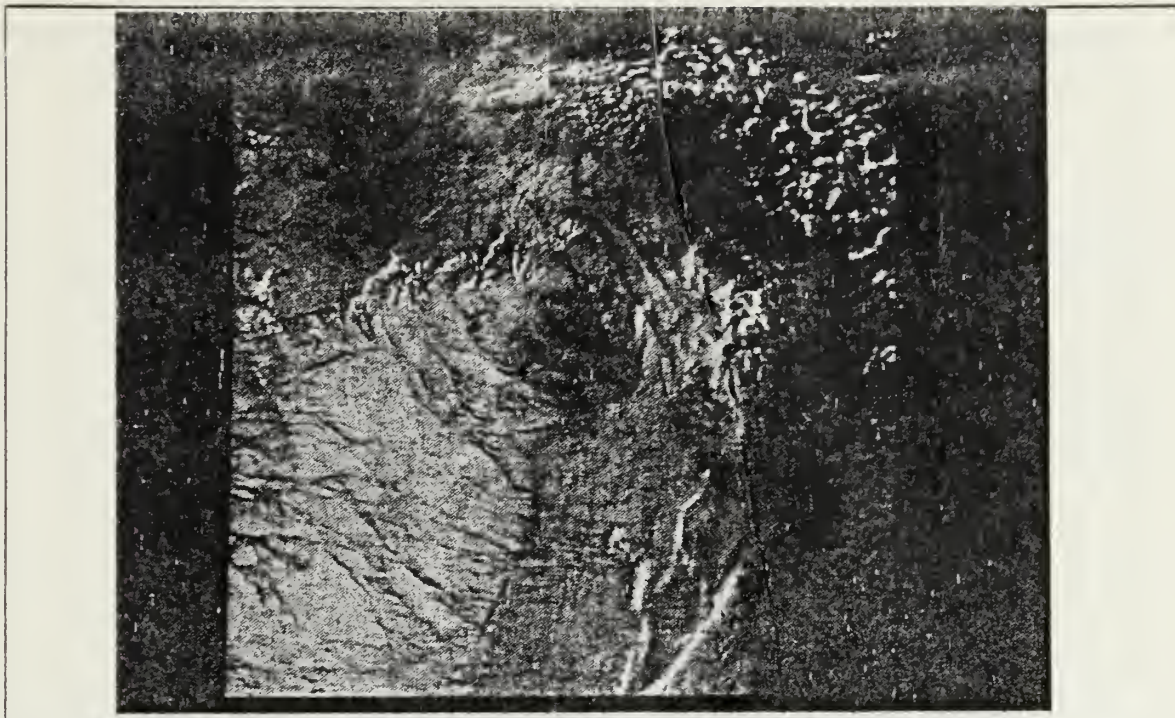
Fig. A.27   Case 6: 1119, 06 Apr 1987, channel 2 subscene.
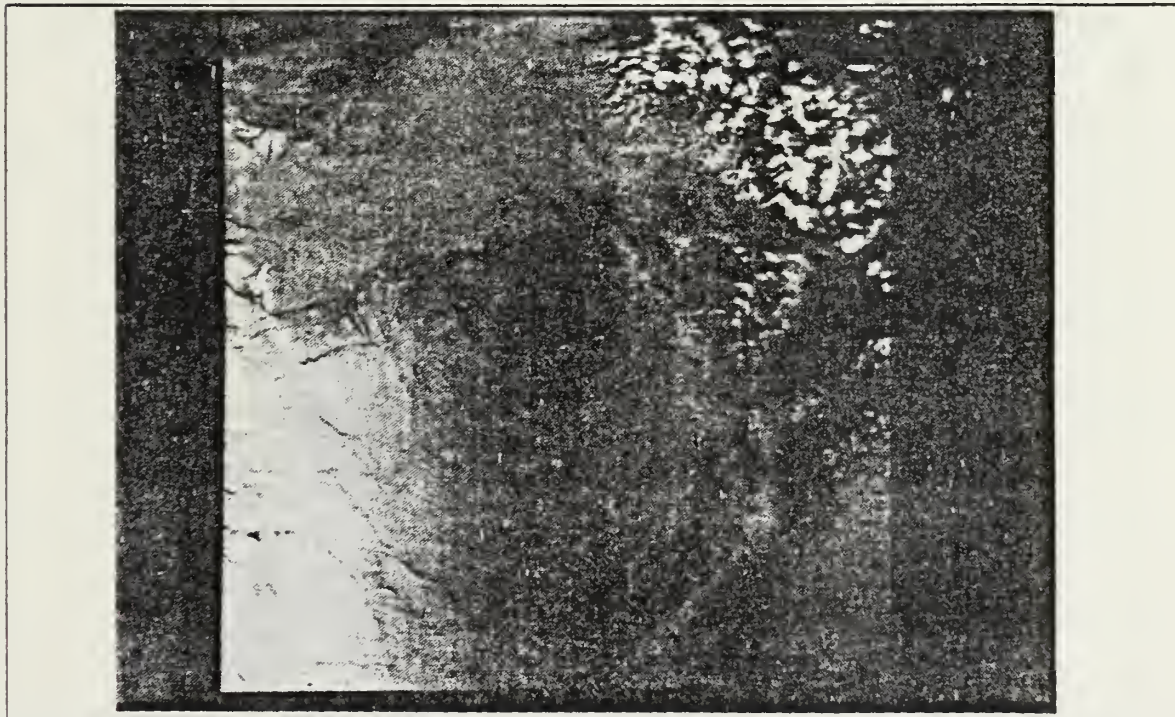
Fig. A.28   Case 6: 1119, 06 Apr 1987, channel 4 subscene.

Fig. A.29   Case 6: 06 Apr 1119, Channel 3 subscene.
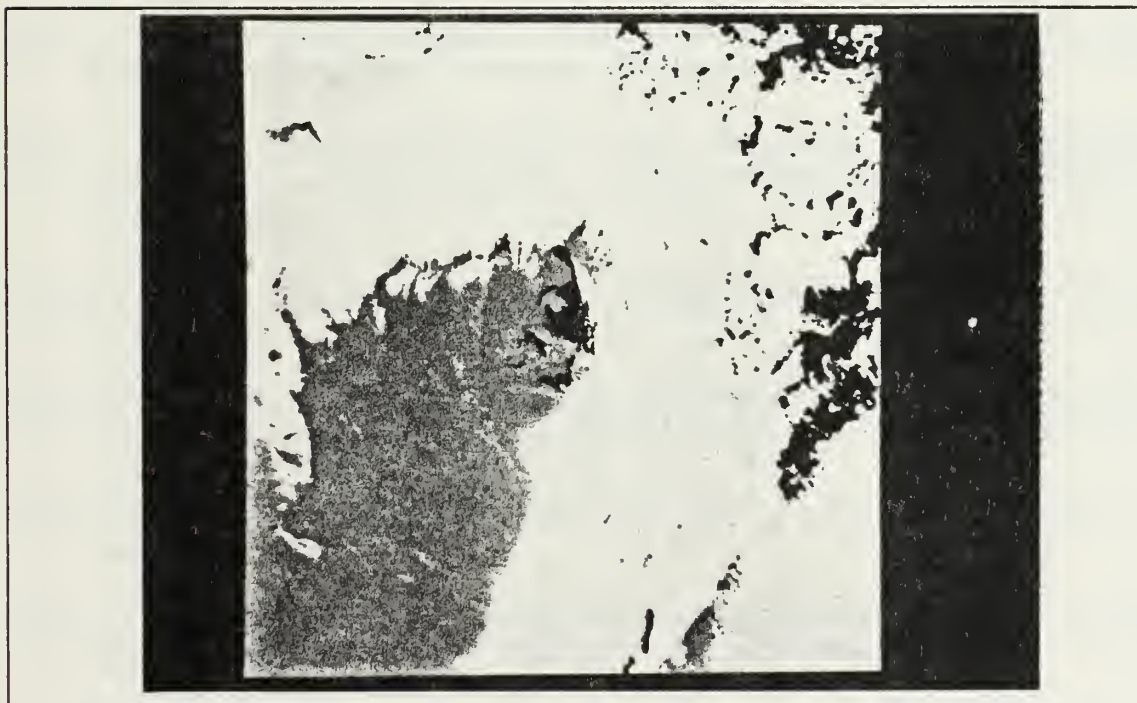
Fig. A.30   Case 6: 06 Apr 1119, Analysis results.

76

LIST OF REFERENCES

Allen, R.C., Jr., 1987: *Automated Satellite Cloud Analysis: A Multispectral Approach to the Problem of Snow/Cloud Discrimination*. M.S. Thesis, Naval Postgraduate School, Monterey, CA, June 1987.

Arking, A., 1987: Spectral albedo of snow, ice and clouds: A short review. *Report of the International Satellite Cloud Climatology Project (ISCCP) Workshop on Cloud Algorithms in the Polar Regions (Tokyo, Japan, 19-21 August 1986)*. World Climate Programme, WMO, Geneva, Switzerland, C.1.1-13.

Arking, A. and J.D. Childs, 1985: Retrieval of cloud cover parameters from multispectral satellite images. *J. Climate Appl. Meteor.*, **24**, 322-333.

Bunting, J.T. and R.P. d'Entremont, 1982: Improved cloud detection utilizing Defense Meteorological Satellite Program near infrared measurements. Air Force Geophysics Laboratory Tech. Rep. 82-0027, Hanscom AFB, MA, 91 pp.

Bunting, J.T., 1986: Personal communication. Air Force Geophysics Laboratory, Hanscom AFB, MA.

Ebert, E., 1987: A pattern recognition technique for distinguishing surface and cloud types in the polar regions. *J. Climate Appl. Meteor.*, **26**, 1412-1427.

Felde, G.W., J.T. Bunting and K.R. Hardy, 1986: Atmospheric remote sensing in the arctic regions. Air Force Geophysics Laboratory Tech. Rep. 87-0128, Hanscom AFB, MA, 10 pp.

Foster, J.L., D.K. Hall and A.T.C. Chang, 1987: Remote sensing of snow. *EOS*, **68** (32), 681-684.

Grenfell, T.C. and D.K. Perovich, 1984: Spectral albedos of sea ice and incident solar irradiance in the southern Beaufort Sea. *J. Geophys. Res.*, **89**, 3573-3580.

Hall, D.K. and J. Martinec, 1985: *Remote Sensing of Ice and Snow*. Chapman and Hall, New York, NY, 189 pp.

Hunt, G.E., 1972: Radiative properties of terrestrial clouds at visible and infra-red thermal window wavelengths. *Quart. J. R. Met. Soc.*, **99**, 346-369.

Kidder, S.Q. and H.-T. Wu, 1984: Dramatic contrast between low clouds and snow cover in daytime 3.7 μm imagery. *Mon. Wea. Rev.*, **112**, 2345-2346.

Lauritson, L., G.J. Nelson and F.W. Porto, 1979: Data extraction and calibration of TIROS-N/NOAA radiometers. NOAA Technical Memorandum NESS 107, U.S. Dept. of Commerce, Washington, D.C., Appendix B.

Raschke, E., 1987: *Report of the International Satellite Cloud Climatology Project (ISCCP) Workshop on Cloud Algorithms in the Polar Regions (Tokyo, Japan, 19-21 August 1986).* World Climate Programme, WMO, Geneva, Switzerland, 12 pp.

Raschke, E., H. Jacobs, H.J. Lutz and U. Steffens, 1987: Cloud analysis of AVHRR data measured over polar regions. *Report of the International Satellite Cloud Climatology Project (ISCCP) Workshop on Cloud Algorithms in the Polar Regions (Tokyo, Japan, 19-21 August 1986).* World Climate Programme, WMO, Geneva, Switzerland, C.6.1-8.

Ruff, I. and A. Gruber, 1983: Multispectral identification of clouds and earth surfaces using AVHRR radiometric data. *Preprints Fifth Conf. on Atmospheric Radiation,* American Meteorological Society, Baltimore, MD, 31 October - 4 November 1983.

Shettle, E.P. and J.A. Weinman, 1970: The transfer of solar irradiance through inhomogeneous turbid atmospheres evaluated by Eddington's approximation. *J. Atmos. Sci.,* **27**, 1048-1055.

Stephens, G.L., 1981: The transfer of 3.7μm radiation through model cirrus clouds. *Preprints Fourth Conf. on Atmospheric Radiation,* American Meteorological Society, Toronto, Ont., Canada, 16-18 June 1981.

Taylor, V.R. and L.L. Stowe, 1984: Atlas of reflectance patterns for uniform earth and cloud surfaces (NIMBUS-7 ERB--61 days). NOAA Tech. Rep. NESDIS 10, U.S. Dept of Commerce, Washington, D.C., 66 pp.

Warren, S.G. and W.J. Wiscombe, 1980: A model for the spectral albedo of snow. II: Snow containing atmospheric aerosols. *J. Atmos. Sci.,* **37**, 2734-2745.

Wiscombe, W.J. and S.G. Warren, 1980: A model for the spectral albedo of snow. I: Pure snow. *J. Atmos. Sci.,* **37**, 2712-2733.

INITIAL DISTRIBUTION LIST

11. Commanding Officer   1
    Fleet Numerical Oceanography Center
    Monterey, CA 93943

12. Commanding Officer   1
    Naval Environmental Prediction Research Facility
    Monterey, CA 93943

13. Chairman, Oceanography Department   1
    U. S. Naval Academy
    Annapolis, MD 21402

14. Chief of Naval Research   1
    800 North Quincy Street
    Arlington, VA 22217

15. Office of Naval Research (Code 420)   1
    Naval Ocean Research and Development Activity
    800 North Quincy Street
    Arlington, VA 22217

16. Lt. Zdenka Willis   1
    Naval Polar Oceanography Center
    4301 Suitland Road
    Washington, DC 20390-5180